International Journal of Concrete Structures and Materials

RESEARCH Open Access

Research on Whole-Process Tensile Behavior of Headed Studs in Steel–Concrete Composite Structures

Liang-Dong Zhuang[1], Hong-Bing Chen[1], Yuan Ma[1] and Ran Ding[1,2*]

Abstract

The headed studs have been widely applied in steel–concrete composite structures as shear connectors. However, the tensile performance of headed studs is also key to the structural performance in many cases such as the semi-rigid composite joints including steel beam–concrete wall joint and steel column–base joint. Therefore, this study presents experimental and analytical study on the whole-process tensile behavior of headed studs. Tests on a total of 33 pullout specimens are first conducted. The tensile capacity and load–deformation behavior of the anchorage concrete, which dominates the structural performance of headed studs, are thoroughly analyzed. In addition, test data in the literature are collected for quantitatively evaluating the influence of embedment depth, bearing area, boundary conditions, and concrete strength on the tensile behavior of the anchorage concrete. On the basis of the influence evaluation, an analytical model represented by a piecewise function is proposed to describe the whole-process load–deformation behavior of the anchorage concrete and validated through the comparison between the predicted curves and all collected experimental results. Then the proposed model is applied to simulate the rotational behavior of the typical semi-rigid joint anchored by headed studs, which takes the contribution of the anchorage concrete into consideration, and is verified by experimental results. The research findings indicate that tensile behavior of anchorage concrete is crucial to the structural performance of semi-rigid joints, even for headed studs with large embedment depth and bearing area.

Keywords: headed studs, tensile behavior, load–deformation curve, anchorage concrete, semi-rigid joint, analytical model

1 Introduction

Headed studs have been widely applied to transfer shear force between steel and concrete members in composite structures such as the composite beams and composite columns. However, with the increasing demand for composite components, various kinds of joints between conventional reinforced concrete and steel–concrete composite structure are developed. As illustrated in Fig. 1, the headed studs play a key role in transferring tensile forces of the beam-to-wall joint and column–base joint. It has been reported that the tensile performance of headed studs may significantly influence the semi-rigid behavior of these composite joints (Derek et al., 2013; Grauvilardell et al., 2005; Latour & Rizzano, 2019) as well as the global performance of the composite structure system (Latour et al., 2014; Pallarés & Hajjar, 2010; Shahrooz et al., 2004). In addition, headed studs used in double-skin steel–concrete composite shear walls are beneficial to prevent the buckling of steel plate (Yang et al., 2016). In this case, headed studs are mainly subjected to tensile force between concrete and steel face plate. Therefore, the structural performance of headed studs and the

*Correspondence: dingran@mail.tsinghua.edu.cn
[1] Key Lab. of Civil Engineering Safety and Durability of China Education Ministry, Dept. of Civil Engineering, Tsinghua University, Beijing 100084, China
Full list of author information is available at the end of the article
Journal information: ISSN 1976-0485 / eISSN 2234-1315

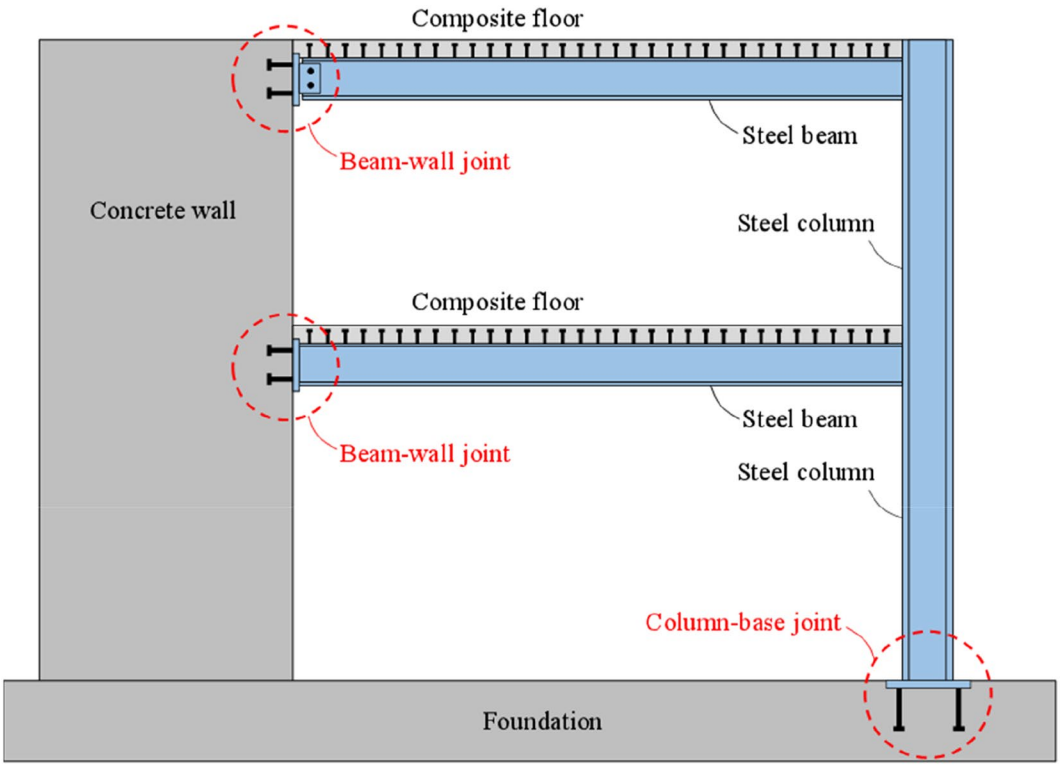

Fig. 1 Headed studs subjected to tensile loading patterns.

transferring mechanism of tensile load need to be investigated in depth.

According to the load transfer mechanism of headed studs proposed by Eligehausen et al., (2006), the tensile performance of headed studs is primarily dependent on the stud shank and the surrounding concrete anchoring the stud (referred as the anchorage concrete). Since the tensile behavior of the stud shank is almost identical to that of the stud shank material without welding fracture, the tensile performance of anchorage concrete becomes a research hotspot in the current stage. The concrete capacity design (CCD) method (Fuchs, 1995), which can predict the tensile strength of headed stud embedded in concrete considering the effects of concrete strength, embedment depth, edge distance, stud spacing, and load eccentricity, has been widely adopted by structural design standards (American Concrete Institute Committee 349 (ACI), 2006; American Concrete Institute Committee 318 (ACI), 2014; Prestressed Concrete Institute (PCI), 2004). Based on the CCD method, recent research aimed to improve the accuracy and extend the range of application of the method (Ožbolt et al., 1999; Lee et al., 2007; Hoehler & Eligehausen, 2008; Piccinin et al., 2010; Henriques et al., 2013; Nilforoush et al., 2017a, 2017b, 2018). Ožbolt et al. (1999) conducted experimental and analytical studies to show that there is a strong size effect on the tensile capacity of headed studs. Lee et al. (2007) investigated the tensile performance of headed studs with large diameter and deep embedment, and the results were used to modify the existing design provision. Hoehler and Eligehausen (2008) experimentally investigated the tensile behavior of headed studs in cracked concrete where the cracks are repeatedly opened and closed. Piccinin et al. (2010) used linear elastic fracture mechanics analysis to reveal the influence of concrete prestress, and the results showed that the increasing of compressive prestress can improve the load-carrying capacity and ductility of the headed studs. Henriques et al. (2013) experimentally evaluated the influence of hanger reinforcement on the tensile behavior of headed studs, and extensive numerical and experimental study was carried out by Nilforoush et al. (2017a, 2017b, 2018) to illustrate the influence of concrete member thickness, anchor-head size, crack conditions and orthogonal surface reinforcement on the tensile capacity.

However, the collected literatures mainly addressed the prediction of the ultimate strength of the anchorage concrete. The characteristics of the whole-process tensile load–deformation behavior of the anchorage concrete under different failure modes were only

qualitatively discussed in few researches (Derek et al., 2013; Eligehausen et al., 1998, 2006; Nilforoush, 2018). Due to the complexity of the failure mechanism of the concrete and the insufficient experimental study, it is generally difficult to propose a quantitative model to describe the whole-process pullout behavior of the anchorage concrete. Thus, the influence of the anchorage concrete to the rotational behavior of the composite joint is commonly ignored (EN, 1993-1-8, 2004; Wald et al., 2008) or simplified as the contribution of an elastic effective concrete cylinder (Tsavdaridis et al., 2016). Then the nonlinear evolution of the pull load with the increase of the damage and cracking of the anchorage concrete cannot be depicted accurately by the simple and practical modeling strategies. Berger (2015) once proposed an analytical model to forecast the nonlinear deformation of the anchorage concrete under the bearing pressure applied by the stud head. However, in Berger's model, it was assumed that the breakout of the concrete cone only contributed to the deformation after reaching the ultimate strength, which is more suitable for the prediction of the load–deformation behavior when pullout failure (see Fig. 2b) happens. The more typical concrete cone breakout failure (see Fig. 2a) can not be reasonably described.

Although accurate predictions can be achieved through the FEM analysis (Chang et al., 2011; Derek et al., 2013; Ottosen, 1981; Ozbolt & Eligehausen, 1993; Ozbolt et al., 2003; Wang et al., 1993), the FEM modeling and analysis on large-scale structural systems are extremely difficult and time-consuming, which are usually accompanied with severe convergence problems. Therefore, to consider reasonably the influence of the nonlinear tensile behavior of head studs on the structural performance, it is necessary to develop an accurate yet simple model to predict the whole-process pullout behavior of the anchorage concrete.

In this study, the load–deformation behavior of the anchorage concrete of headed studs is first experimentally investigated. A total of 33 pullout tests with different embedment depths, bearing areas and boundary conditions are conducted. Based on the test observations, an analytical model considering the stiffness and strength degradation of the anchorage concrete is proposed to describe the tensile load–deformation behavior of anchorage concrete. The load–deformation curves of test specimens in this study, along with 37 load–deformation curves collected from reported tests, are analyzed to determine the characteristic parameters in the proposed model. Furthermore, the accuracy of the proposed function is verified by comparing predicted results with experimental results obtained from the pullout tests with different design parameters and column–base joint tests. Finally, the significance of considering the nonlinear tensile behavior of the anchorage concrete is addressed and design suggestions are provided.

2 Experimental Investigation

2.1 Test Program

In this section, a total of 33 pullout specimens are designed and tested using monotonic tensile loading pattern. The geometrical parameters of tested specimens including the embedment depth h_{ef}, shoulder width of the stud head a, edge distance C_a, stud number n and stud spacing S are summarized in Table 1. Specimens No. 1–10 are tested to evaluate the influence of embedment depth and bearing area. Specimens No. 11–22 and Specimens No. 23–33 are designed to assess the influence of boundary conditions including the free edge conditions and group studs conditions, respectively.

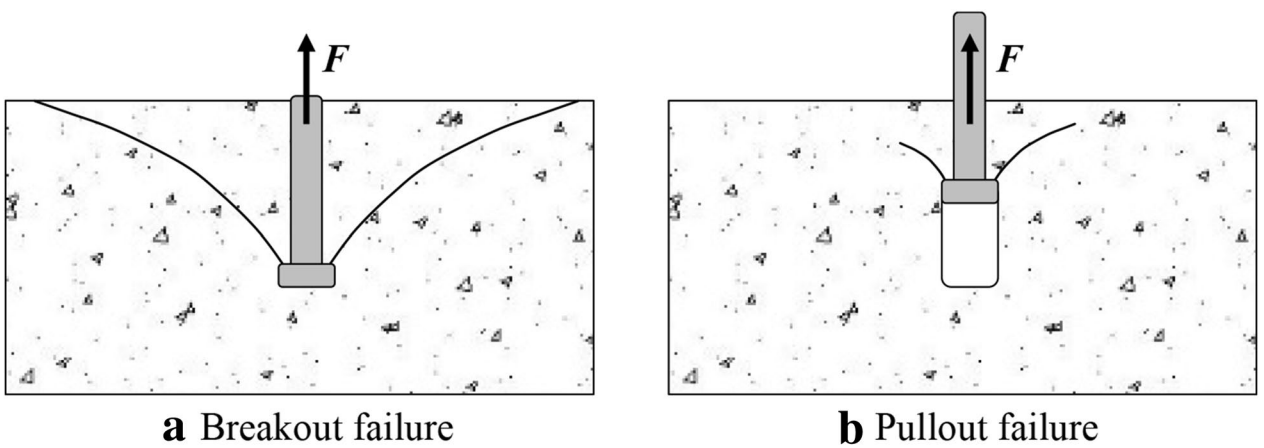

Fig. 2 Failure modes of the anchorage concrete.

Table 1 Geometrical parameters of test specimens (Unit: mm).

No	h_{ef}	a	n_s	Layout pattern	No	h_{ef}	a	n_s	Layout pattern
1	120	6.5	1	Centered	17	170	6.5	1	One edge, C_a=80
2	120	6.5	1	Centered	18	170	6.5	1	One edge, C_a=80
3	120	6.5	1	Centered	19	170	6.5	1	One edge, C_a=80
4	170	6.5	1	Centered	20	170	6.5	1	Two edge, C_a=80
5	170	6.5	1	Centered	21	170	6.5	1	Two edge, C_a=80
6	170	6.5	1	Centered	22	170	6.5	1	Two edge, C_a=80
7	80	10.5	1	Centered	23	120	6.5	2	Straight, S=120
8	80	20.5	1	Centered	24	120	6.5	2	Straight, S=180
9	120	10.5	1	Centered	25	120	6.5	2	Straight, S=240
10	120	20.5	1	Centered	26	120	6.5	3	Straight, S=120
11	120	6.5	1	One edge, C_a=60	27	120	6.5	3	Straight, S=180
12	120	6.5	1	One edge, C_a=60	28	120	6.5	3	Straight, S=240
13	120	6.5	1	One edge, C_a=60	29	120	6.5	4	Square, S=120
14	120	6.5	1	Two edge, C_a=60	30	120	6.5	4	Square, S=180
15	120	6.5	1	Two edge, C_a=60	31	170	6.5	2	Straight, S=180
16	120	6.5	1	Two edge, C_a=60	32	170	6.5	3	Straight, S=180
					33	170	6.5	4	Square, S=180

h_{ef} represents the embedment depth of the headed stud; a represents the shoulder width of the stud head; n_s represents the number of headed studs; C_a represents the edge distance of the stud; S represents the distance between studs.

A total of five types of layout patterns are adopted in the test specimens, as shown in Fig. 3a. For a centered layout, single stud is anchored with an edge distance larger than $2.0h_{ef}$, to exclude the edge effect, according to ACI 318-14 (American Concrete Institute Committee318, 2014). For the one-edge or two-edge layout, single stud is anchored with the presence of one or two free edges located at a distance of C_a to the stud center. For the straight layout, two or three studs are evenly distributed in line with a spacing of S. For the square layout, four studs are arranged at the corners of a square region with a side length of S. In practice, there are a number of possible geometrical combinations, which are not covered by this test program. For example, it is possible to design headed studs anchored in concrete where the edge distances of four sides are all less than $2.0h_{ef}$. However, since they are not as usual as cases considered in this study and the number of test

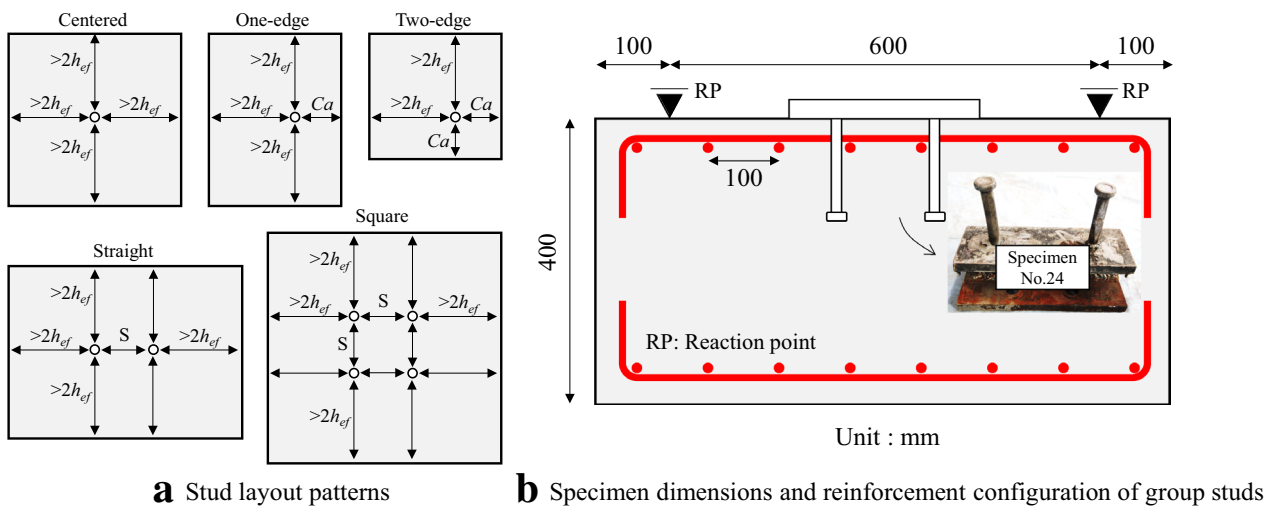

Fig. 3 Specimen design details.

specimens is limited, these special conditions are not included in Table 1.

2.2 Specimens Design

The dimension of the anchorage concrete is illustrated in Fig. 3b. To prevent the potential splitting failure of group studs due to the flexural cracking of the anchorage concrete under the vertical pulling loads, 12-mm-diameter steel reinforcement bars is uniformly distributed at the top and the bottom of anchorage concrete with a spacing of 100 mm. The steel reinforcement bars were made of HRB 400 (CMC, 2010) with yielding strength $f_{yk} = 400$ MPa.

To obtain the actual concrete strength of the specimens, 200 × 200 × 200 mm concrete cubes were cast. The obtained compressive strength of the concrete f_{cc} at the time of testing is averagely 42.8 MPa with a standard deviation of 2.1 MPa. The specimens are designed to fail in brittle failure modes accompanying with the breakout of the anchorage concrete. Therefore, headed studs are designed with a sufficient yielding strength to prevent premature failure. According to the manufacturer's specification on the standard 19-mm-diameter headed studs, the elastic modulus E_s and yielding strength f_s are 208 GPa and 635MPa, respectively.

2.3 Test Setup and Instrumentation

As shown in Fig. 4, a self-balanced loading system, which is composed of a reaction frame placed on the test specimen and the center-hollowed jack seated on the frame, is designed for experimental study. The loading pole of the jack is connected with the top flange of a short transferring beam through four stiff bolts. To eliminate the influence of load eccentricity, four LVDTs are arranged at the corners of the bottom flange of the transferring beam, the average value of the recorded data of the LVDTs is adopted as the deflection of the specimen. According to the design suggestions in the standards ACI 318-14, the boundaries of the concrete have few effects on the pullout behavior of headed stud, when the distance between the headed stud and the boundaries is larger than $1.5h_{ef}$. In the design of the experimental setup, the position of the column of the reaction frame is adjusted so that the distance between the headed stud and the edge of the column–base is larger than $1.5h_{ef}$, which can help to prevent the influence of the reaction zone of the test setup on the deformability of the test specimen.

Figure 5 shows the deformation components of headed stud under tension load. It can be seen that the deformation of headed stud can be separated into two parts simultaneously. First, the stud shank would deform linearly with the increase of pullout load before yielding, and the deformation can be determined as $(P \cdot h_{ef}) / (n_s \cdot E_s \cdot A_d)$, where P is the applied pulling load and A_d is the sectional area of the stud shank. Second, the anchorage concrete would deform under the bearing pressure transmitted by the stud head. The deformation is composed of

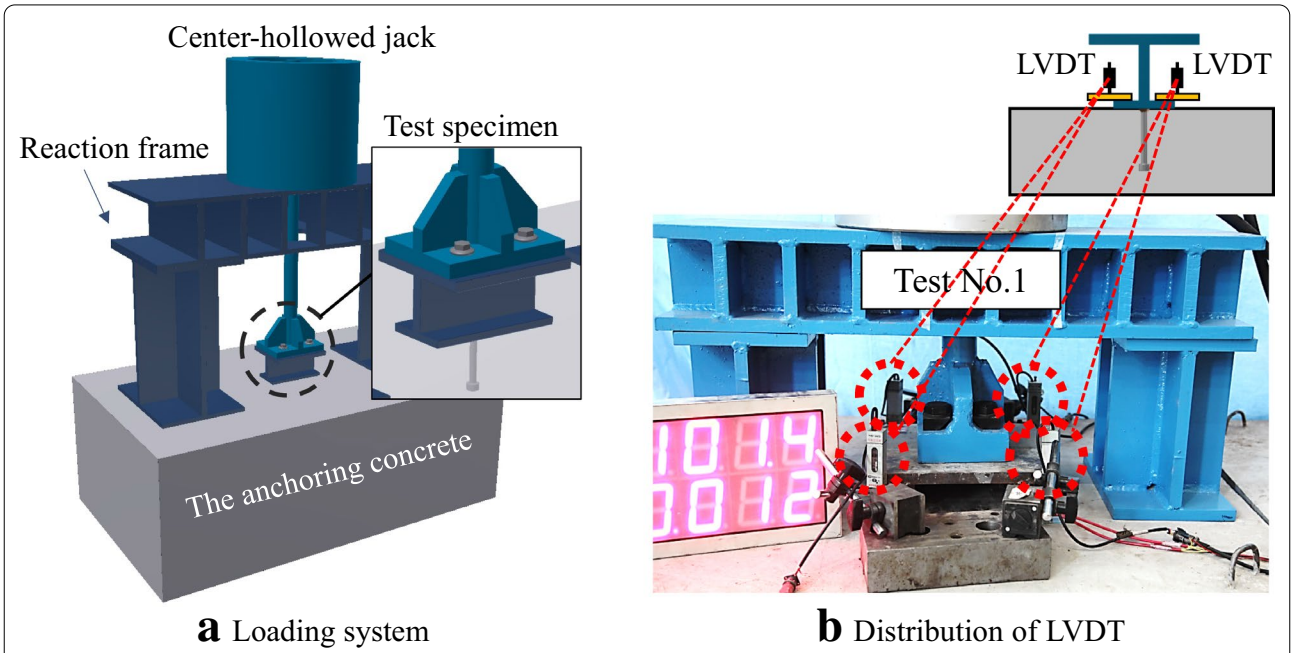

Fig. 4 Test setup and instrumentation.

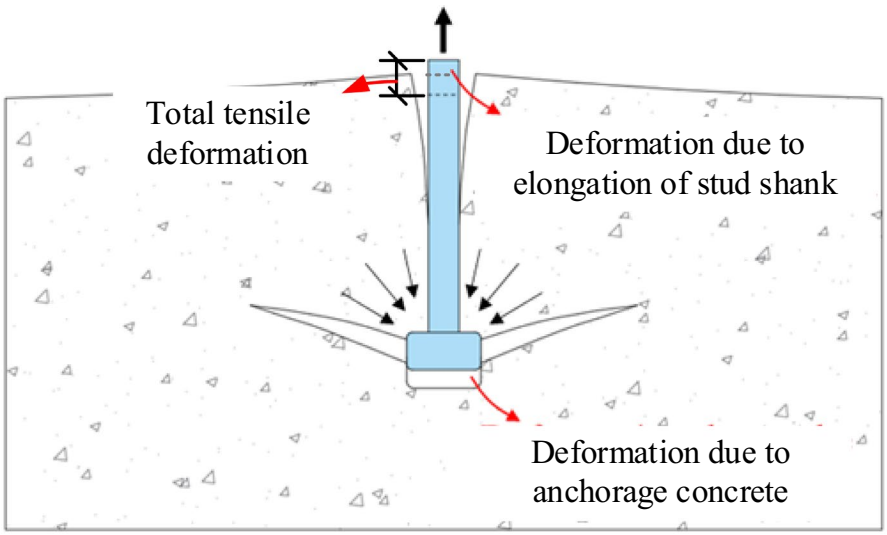

Fig. 5 Deformation components analysis of the headed stud.

the compressive deformation of the local concrete near stud head and the crack width of the breakout block. Since these two deformation components are inside the anchorage concrete and are hard to measure, the deformation of the concrete is obtained by subtracting the deformation of the stud shank from the total tensile deformation of the specimen measured by the LVDTs.

2.4 Test Results and Discussion

The typical failure patterns observed in the tests are exhibited in Fig. 6. The failure mode of the anchorage concrete with large bearing area is mainly dominated by the breakout failure of the concrete cone, as shown in Fig. 6a. When headed studs are anchored in the concrete with smaller bearing area or subjected to free edges, the breakout concrete is likely to split into pieces, presenting the radial cracks initiating from the center of the anchorage concrete, as shown in Fig. 6b, c. Since the bending stress at the surface of the breakout cone may exceed the tensile strength of the concrete due to stress concentration near the stud hole, flexural cracks may initiate, propagate, and finally separate the breakout concrete, which happens before the complete formation of the breakout cone. For the test specimens with group studs spacing less than $1.5h_{ef}$, the breakout of group studs can be observed in all specimens, as illustrated in Fig. 6d. In addition, Fig. 6e shows that large deformation is clearly visible in the surface reinforcement, indicating that the surface reinforcement can effectively restrain the breakout failure of group studs. With the increment of the embedment depth and stud spacing, the restraint provided by the surface reinforcement has become more significant, as shown in Fig. 6f, where the upper reinforced layer of the anchorage concrete could be entirely uplifted with the breakout of group studs. All test results of failure patterns and maximum load (N_u) are summarized in Table 2, and the load–deflections curves of the anchorage concrete can be found in Additional file 1: Appendix B.

Figure 7a shows the decomposition of the total displacement of a typical specimen (No. 1) before reaching the maximum loading level. It can be clearly seen that the contribution of the deflection of the anchorage concrete to the total displacement is gradually increasing with the increment of the applied load and almost dominates the deformation when reaching the maximum load. Since the stud shank is always kept elastic during loading, the nonlinear characteristics of the load–deformation behavior of the headed studs are entirely controlled by the deformation response of the anchorage concrete. For further comparison, the ratio of the anchorage concrete deformation to the total displacement with the development of the applied load normalized by the corresponding maximum load is summarized in Fig. 7b. When designed with different embedment depths, bearing areas and boundary conditions, the anchorage concrete contributes to 10–71% (47% in average) of the total displacement of the specimen at 50% of the maximum load and the contribution ratio reaches even 37–86% (72% in average) at the maximum loading level. For most of headed studs, their load–deformation behavior is dominantly controlled by the anchorage concrete. However, there are a few specimens whose deformation characteristics are less relevant with the anchorage concrete. For example, in specimen

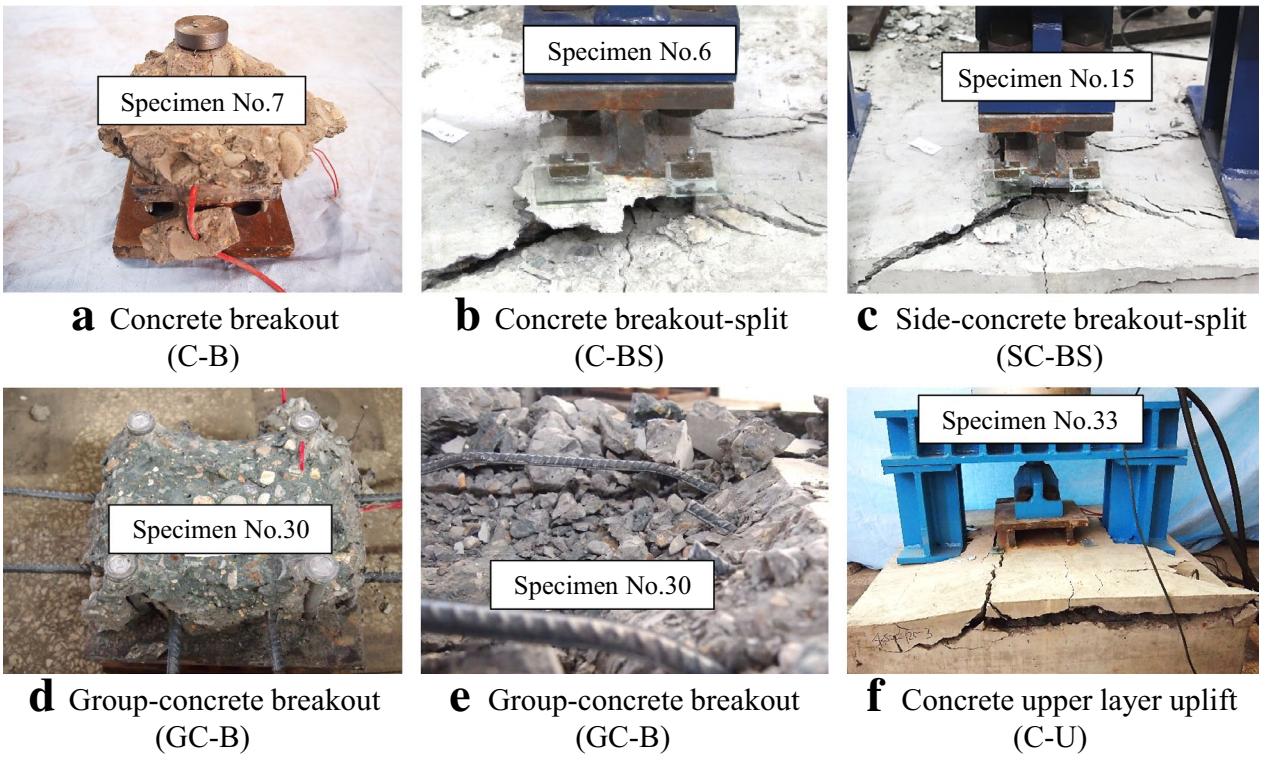

Fig. 6 Typical failure patterns.

Table 2 Test results (Unit: kN).

No	N_u	Failure pattern	No	N_u	Failure pattern	No	N_u	Failure pattern
1	137	C-BS	12	96	SC-BS	23	196	GC-B
2	138	C-BS	13	108	SC-BS	24	229	GC-B
3	136	C-BS	14	68	SC-BS	25	229	GC-B
4	179	C-BS	15	96	SC-BS	26	252	GC-B
5	178	C-BS	16	98	SC-BS	27	290	C-U
6	137	C-BS	17	129	SC-BS	28	280	C-U
7	64	C-B	18	141	SC-BS	29	240	GC-B
8	74	C-B	19	121	SC-BS	30	345	GC-B
9	113	C-B	20	142	SC-BS	31	231	GC-B
10	124	C-B	21	128	SC-BS	32	400	C-U
11	91	SC-BS	22	113	SC-BS	33	460	C-U

N_u represents the ultimate strength of the anchorage concrete; "C-BS" means the concrete breakout-split failure; "C-B" means the concrete breakout failure; "SC-BS" means the side-concrete breakout failure-split failure; "GC-B" means the group-concrete breakout failure; "C-U" means the concrete upper layer uplift failure.

No. 8 and No. 9 which have a large head bearing area compared with other specimens, the contribution of the anchorage concrete to the deformation of the head stud is less than 20% when reaching 50% of the maximum load, but the contribution also exceeds 37% at the maximum load. Therefore, a proper design may reduce the influence of anchorage concrete on the total deformation of headed stud, but the deformation of the anchorage concrete is always an important factor which should be accounted for in design.

The typical load–deformation curve of the anchorage concrete is plotted for specimen No. 1 in Fig. 8. The load–deformation curve can be divided as the ascending stage, critical stage and failure stage. In the ascending stage, the deformation is linearly increasing with the applied load due to the elastic compression of the local concrete above

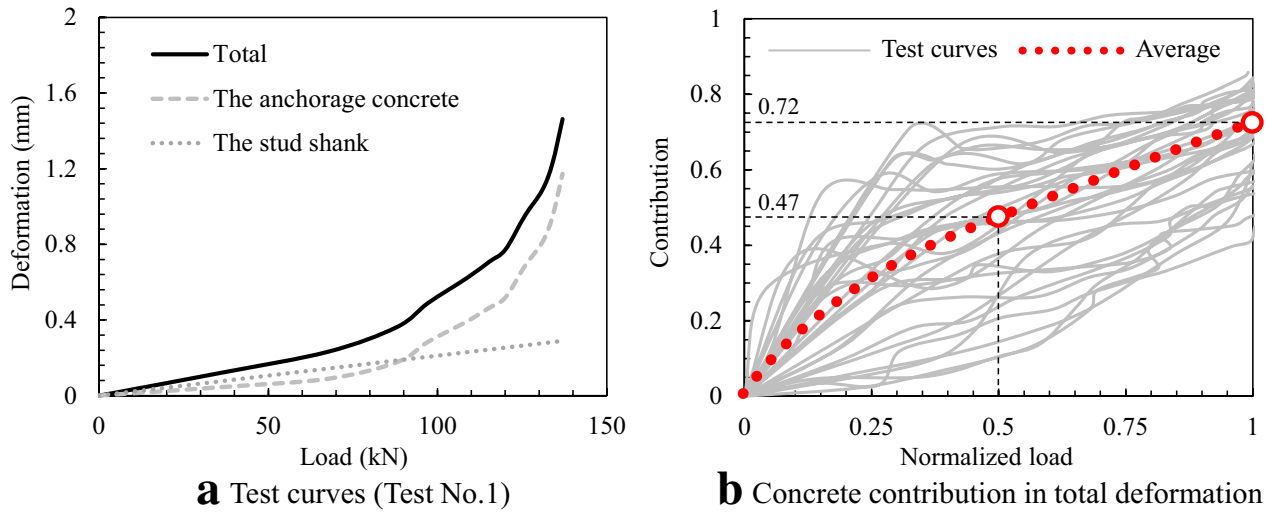

Fig. 7 Contribution of the anchorage concrete to the tensile deformation of headed studs.

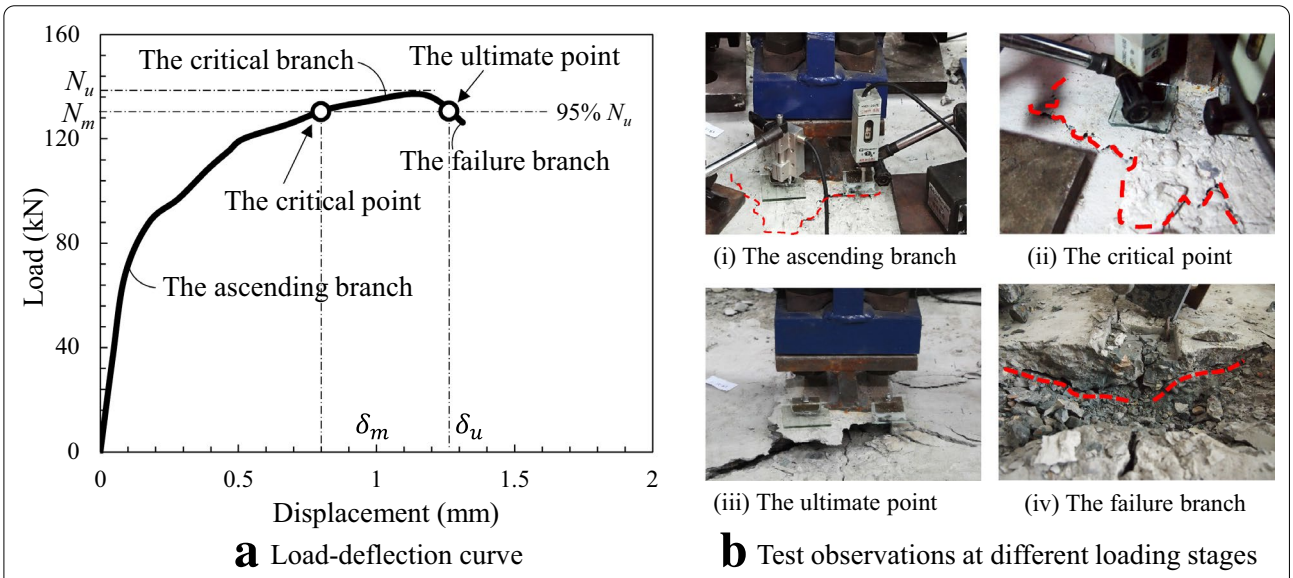

Fig. 8 Load–deformation behavior of the anchorage concrete (Specimen No.1).

the bearing area of the stud head. However, a gradual loss of anchorage stiffness is observed in the anchorage concrete after the crushing of the local concrete in the presence of small bearing area or the cracking initiated from the edge of the stud head. After that, the deformation has obviously accelerated with the increase of the applied load. In the critical stage, significant development of the circumferential cracking of the breakout concrete occurs and the deformation is rapidly increasing with the propagation of the cracks towards the concrete surface. The failure stage is defined according to loading level when the anchorage capacity starts to descend until a complete breakout of the concrete. For the convenience of quantitatively describing the load–deformation behavior of the anchorage concrete and evaluating the influence of different design parameters, the point corresponding to 95% of N_u is conservatively defined as the critical point of the load–deformation curves separating the ascending stage and critical stage. The characteristic point where the applied load declines to 95% N_u is defined as the failure point to distinguish the critical stage and failure stage.

Significant increase of deformation is observed in tests after reaching 95% N_u due to the cracking of the breakout concrete. Therefore, the 0.95 N_u is specified as the characteristic points of the load–deflection curves instead of the N_u. In addition, the variability of 95% N_u in recorded test data are much lower with contrast to that of the N_u. Comparatively, the 95% N_u is more suitable for quantitatively evaluating the load–deformation behavior of the anchorage concrete.

Furthermore, to investigate the characteristics of the curves in each stage, the load–deformation curves of the anchorage concrete are turned into the normalized load–deformation curves, in which, the normalized load is the ratio of applied load to the load at the critical point (referred as the critical load, N_m, which equals to 95% N_u), and the normalized deformation is the ratio of the actual deformation to the deformation at the critical point (referred as the critical deformation, δ_m). By this mean, the load–deformation behavior of the anchorage concrete can be predicted once the N_m, δ_m, and mathematical expression for the normalized curves are determined. In the following sections, the influencing design parameters will be intensively analyzed based on the experimental results from the test specimens in this study and typical test results from collected literatures.

2.4.1 Influence of Embedment Depth hef

The load–deformation curves of the anchorage concrete with different embedment depths are compared in Fig. 9a, b. The test data of specimen No. 6 are excluded due to the influence of a preliminary crack before loading. Figure 9a, b indicates that the increase of embedment depth can effectively increase the critical load and the critical deformation, due to the fact that a deeper embedment needs higher applied load and deformation to provide enough energy for the formation of the breakout concrete cone. According to the normalized curves shown in Fig. 9c, d, the curve shape in the ascending stage is not very sensitive to the variation of embedment depth. However, after the critical point, the normalized curves presented significantly higher degree of variation due to the brittle failure of the concrete.

The load–deformation behavior of the anchorage concrete with much larger embedment depth is also evaluated through the comparison of test specimens with different dimensions by Bouska (1992). Here, the h_{ef}s are 150 mm and 450 mm, respectively, as shown in Fig. 9e, f. In accordance with the condition with smaller embedment, similar conclusions can be drawn that the critical load and critical deformation are obviously affected by the embedment depth. In contrast, the shape of the normalized load–deformation curves is relatively insensitive to the variation of the embedment depth.

2.4.2 Influence of Bearing Area Ah

Figure 10 shows the comparison of load–deformation behavior of anchorage concrete with different bearing areas. Limited increment of the critical load induced by the increase of bearing area will lead to significant reduction in the critical deformation. For example, when the shoulder width of the stud head is increased from 10.5 mm (Specimen No. 7, $A_h = 973$ mm^2) to 20.5 mm (Specimen No. 8, $A_h = 2543$ mm^2), the average critical load merely increases by 16% while the critical deformation decreases by 57%. This reduction of critical deformation is because the local bearing pressure of the anchorage concrete is reduced when the bearing area of the stud head is increased. Through the comparison of the normalized curves, the influence of the bearing area on the shape of the normalized curves is also neglectable.

In addition, further reduction of the shoulder width of the stud head will result in the significant local concrete crushing under the bearing area, presenting the failure pattern with the pull-through of the anchorage concrete (Furche, 1994). Therefore, the characteristics of the load–deformation curves of the anchorage concrete with extremely smaller bearing area should be studied. In this section, the specimens with a shoulder width ranging from 0.5 mm to 4.0 mm (Furche, 1994) are selected for comparative analysis and the typical load–deformation curves of the anchorage concrete with extremely small bearing area is illustrated in Fig. 11.

It can be seen that with the shoulder of the stud head a decreasing from 4.0 to 0.5 mm, the critical load is significantly reduced by approximately 60% and the critical deformation increased to 14.5 times higher. Nevertheless, the influence of the extremely small bearing area on the shape of the normalized curves is still limited. And the curve shapes after the critical point still show obvious variability due to the brittle concrete failure.

2.4.3 Influence of Boundary Conditions

According to CCD method, the effects of the boundary conditions need to be considered if the edge distance C is less than 1.5 h_{ef} in the presence of free edges or the stud spacing S is less than 3.0 h_{ef} in the presence of group studs. To consider the influence of boundary conditions, the ratio of the projected failure area (A_{Nc}) to the total projected failure area (A_{Nco}) of single stud is recommended in the CCD method to modify the breakout capacity of the anchorage concrete.

Herein, to further evaluate the influence of boundary conditions on the anchorage concrete with single stud, the boundary coefficient Ψ_c is defined, as shown in Eq. (1). The detailed calculation of A_{Nc} and A_{Nco} has been illustrated in the design standards (American Concrete Institute Committee 318 (ACI) 2014):

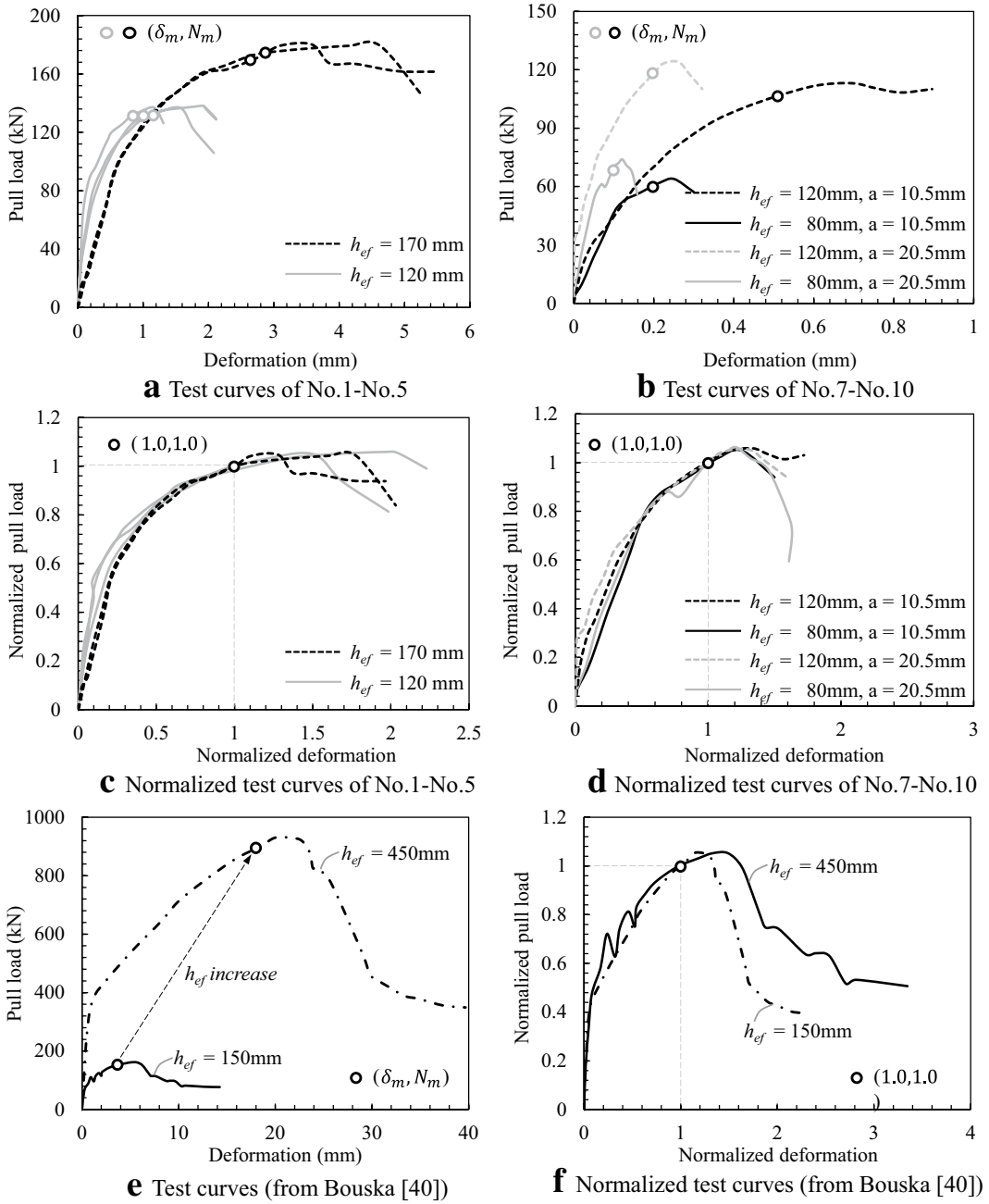

Fig. 9 Load–deformation curves of the anchorage concrete with different embedment depths.

$$\psi_c = \frac{A_{Nc}}{n_s \cdot A_{Nco}} \leq 1.00. \quad (1)$$

The load–deformation curves of the anchorage concrete for a single stud near the free edges or in a group studs arrangement are plotted in Fig. 12. It can be seen that the critical load and critical deformation of the anchorage concrete will reduce significantly while considering the edge effect and group effect of headed stud. However, the critical deformation is even more sensitive to the boundary effects. Taking Fig. 12d as an example, the ratio of the affected critical load to the unaffected case is 0.64 (Ψ_c=0.56) and 0.44 (Ψ_c=0.44), respectively, which agrees well with the prediction of the CCD method that the capacity of the concrete is proportional to the value of Ψ_c. Meanwhile, the ratio of the

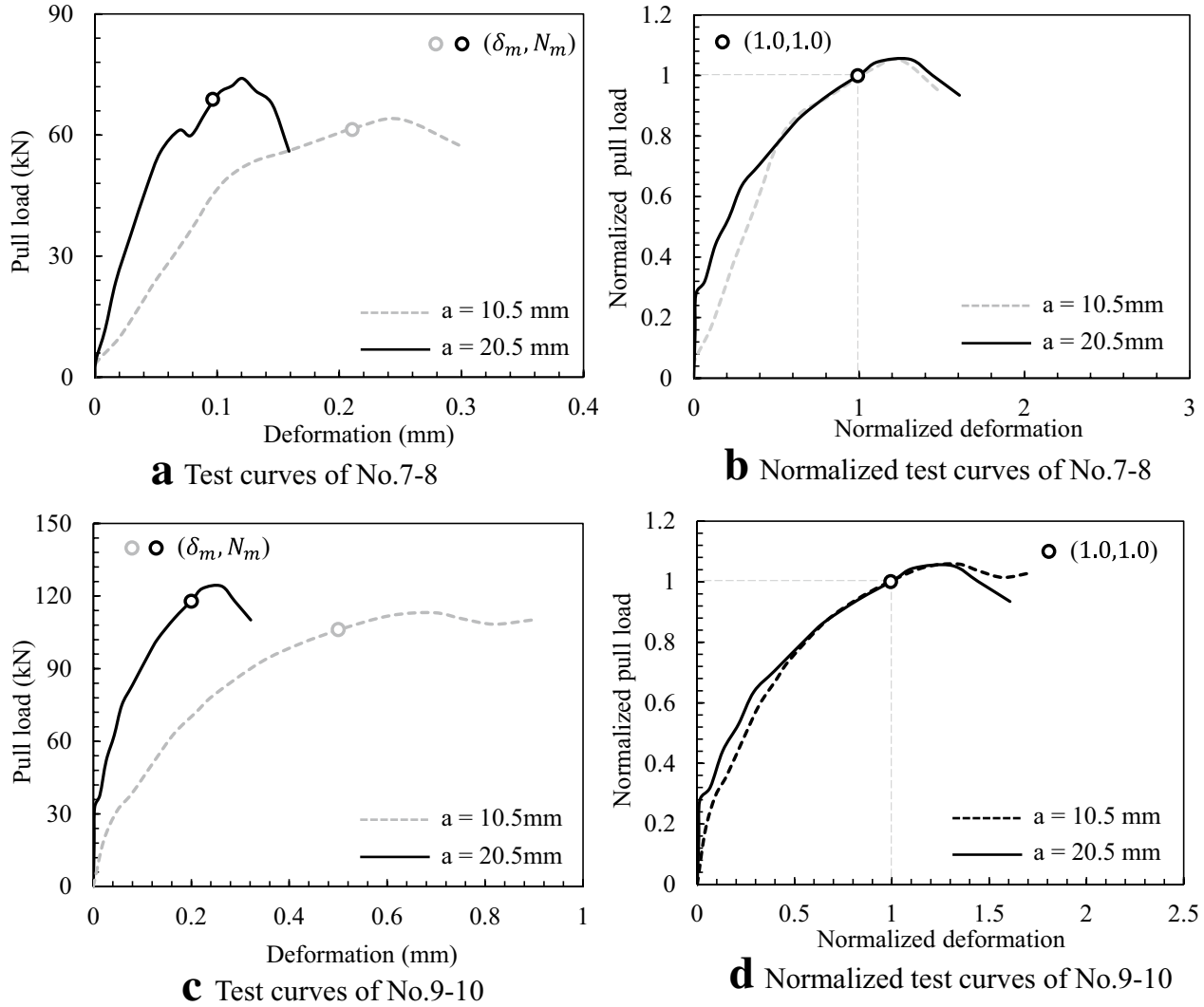

Fig. 10 Load–deformation curves of the anchorage concrete with different bearing areas.

affected critical deformation to the unaffected case is, respectively, 0.31 ($\Psi_c = 0.56$) and 0.14 ($\Psi_c = 0.44$), significantly exceeding the decreasing rate of the critical load.

The normalized curves of the anchorage concrete with different boundary conditions are summarized in Fig. 13. Similar to the conclusions drawn in the discussion on the characteristics of normalized curves with different embedment depths h_{ef} and bearing areas A_h, the descending branches of normalized load–deformation curves still show significant variability. Besides, the curve shapes in the ascending stage show similar patterns and the influence of the boundary conditions on its shape is relatively small.

2.4.4 Influence of Concrete Strength fcc

The improvement of the concrete strength can effectively reduce the compressive deformation of the local concrete under the stud head and postpone the cracking of the breakout concrete, thereby increases the critical load and critical deformation of the anchorage concrete. This deduction can be verified by the tests on the headed studs in the concrete with different strengths (Furche, 1994; Furche & Dieterle, 1986). As shown in Fig. 14, the critical load and the critical deformation are reduced by 14% and 19%, respectively, while the concrete strength increases from 30.0 to 33.4 MPa. Similar to the aforementioned design parameters, the influence of concrete strength on shapes of the normalized curves is also negligible.

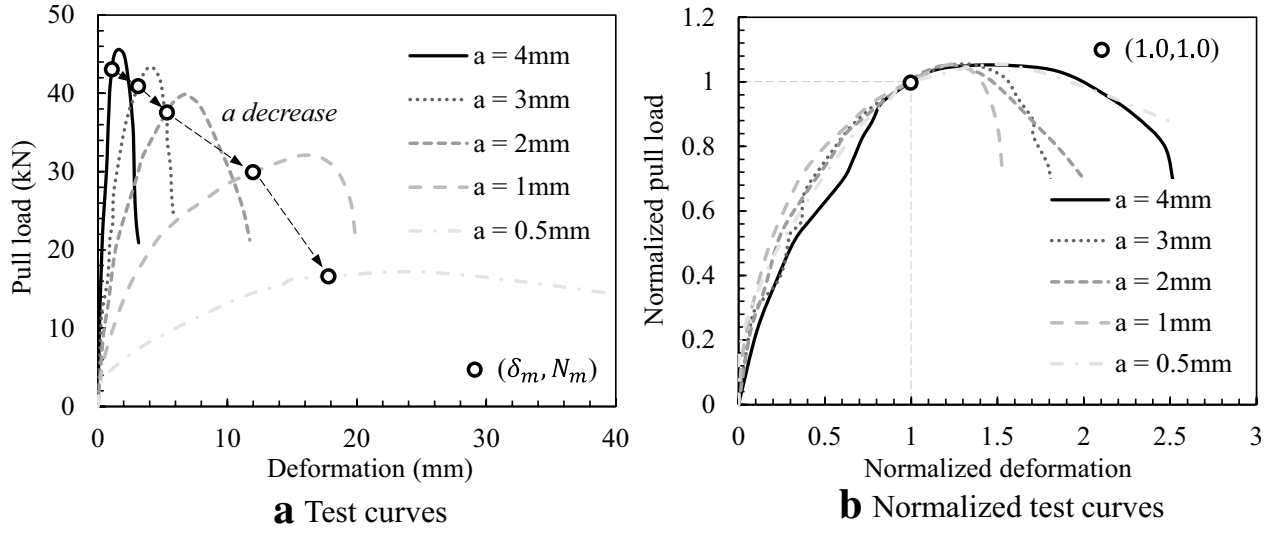

Fig. 11 Typical load–deformation curves of anchorage concrete with extremely small bearing area.

3 Development of Analytical Model for the Tensile Behavior of Anchorage Concrete

To develop the analytical model which can accurately describe the tensile behavior of anchorage concrete, a total of seventy load–deformation curves are collected from the tested specimens in this study and experimental studies performed by other researchers. The detailed information of the investigated design parameters is summarized in Table 3. The load–deformation curves from tested specimens in which the failure is dominated by that of the stud shank or welding fracture are omitted. Besides, the experiment data corresponding to the failure induced by the crushing or splitting of side concrete which is not typical failure patterns of practical headed studs is also excluded by limiting the edge distance or stud spacing according to design provisions (American Concrete Institute Committee 318 (ACI) 2014). Based on the collected load–deformation curves, the critical load N_m, critical deformation δ_m and mathematical expression for the normalized curves are defined and the analytical model for the tensile behavior of anchorage concrete is developed.

3.1 Determination of Critical Load N_m

As discussed in Sect. 2.4, the critical load (N_m) is taken as 95% of the maximum load of the anchorage concrete (N_u) and the N_u stands for the concrete breakout strength calculated as per the modified CCD method specified in ACI 318–14 which includes the effects of deep embedment. The detailed calculation formulas are described as Eqs. (2) and (3). $\Psi_{ed,N}$ is the modification factor considering the influence of asymmetric stress distribution in the presence of free edges (Fuchs, 1995):

$$N_{\mathrm{m}} = 0.95 N_{\mathrm{u}} \Psi_{\mathrm{h}} \tag{2}$$

$$N_u = n_s \Psi_c \Psi_{ed,N} N_b = \begin{cases} 15.5\sqrt{f_{cc}} h_{ef}^{1.5}, h_{ef} < 280mm \\ 5.61\sqrt{f_{cc}} h_{ef}^{1.68}, h_{ef} \geq 280mm \end{cases} \tag{3}$$

$$\Psi_{\mathrm{h}} = 0.171 \ln(A_{\mathrm{h}}) + 0.036 \leq 1.20. \tag{4}$$

The ratio of the test strength to the predicted strength with different bearing areas is presented in Fig. 15a. It can be seen that the prediction curve calculated with Eq. (3) apparently overestimates the strength of the anchorage concrete under small bearing area since the pull-through of headed studs may occur during the early stage of loading which will further reduce the effective embedment depth. Meanwhile, the strength corresponding to large bearing area will be underestimated by Eq. (3) due to the fact that large bearing area could increase cracking surface of the breakout concrete.

Therefore, a modification factor (Ψ_h) considering the influence of the bearing area A_{h} (mm^2) is proposed, as illustrated in Eq. (4). Ψ_h is determined according to the fitted trend line for the discrete points in Fig. 15a, representing the development tendency of prediction error with bearing area. When the bearing area is relatively small, test strength would increase sharply with the increase of bearing area; therefore, a logarithmic function is used in the trend line to depict such tendency. In addition, with the continuous increase of bearing area, its influence on the strength of the anchorage concrete

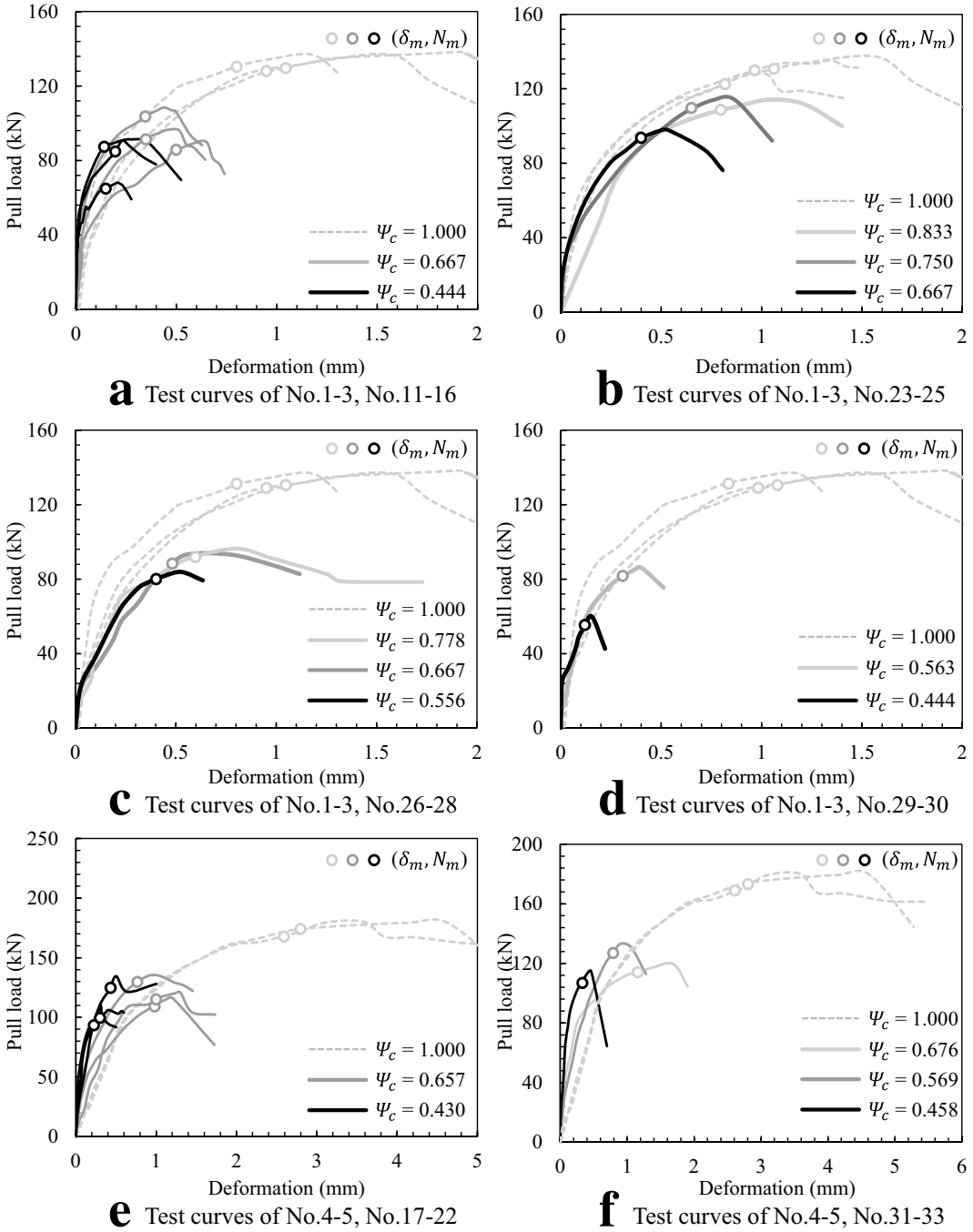

Fig. 12 Load–deformation curves of the anchorage concrete with different boundary conditions.

becomes weak. Therefore, a horizontal line segment is used for convenience. When the maximum value of Ψ_h is 1.20, the average ratio of the test strength to modified predicted strength can be reduced from 1.11 to 1.00 and the corresponding standard deviation (STD) can decrease from 0.31 to 0.15, as shown in the comparison between Fig. 15a, b.

Furthermore, Fig. 15c plotted the influence of peak bearing pressure at the stud head on the ratio of test strength to predicted strength modified by Eq. (4). The

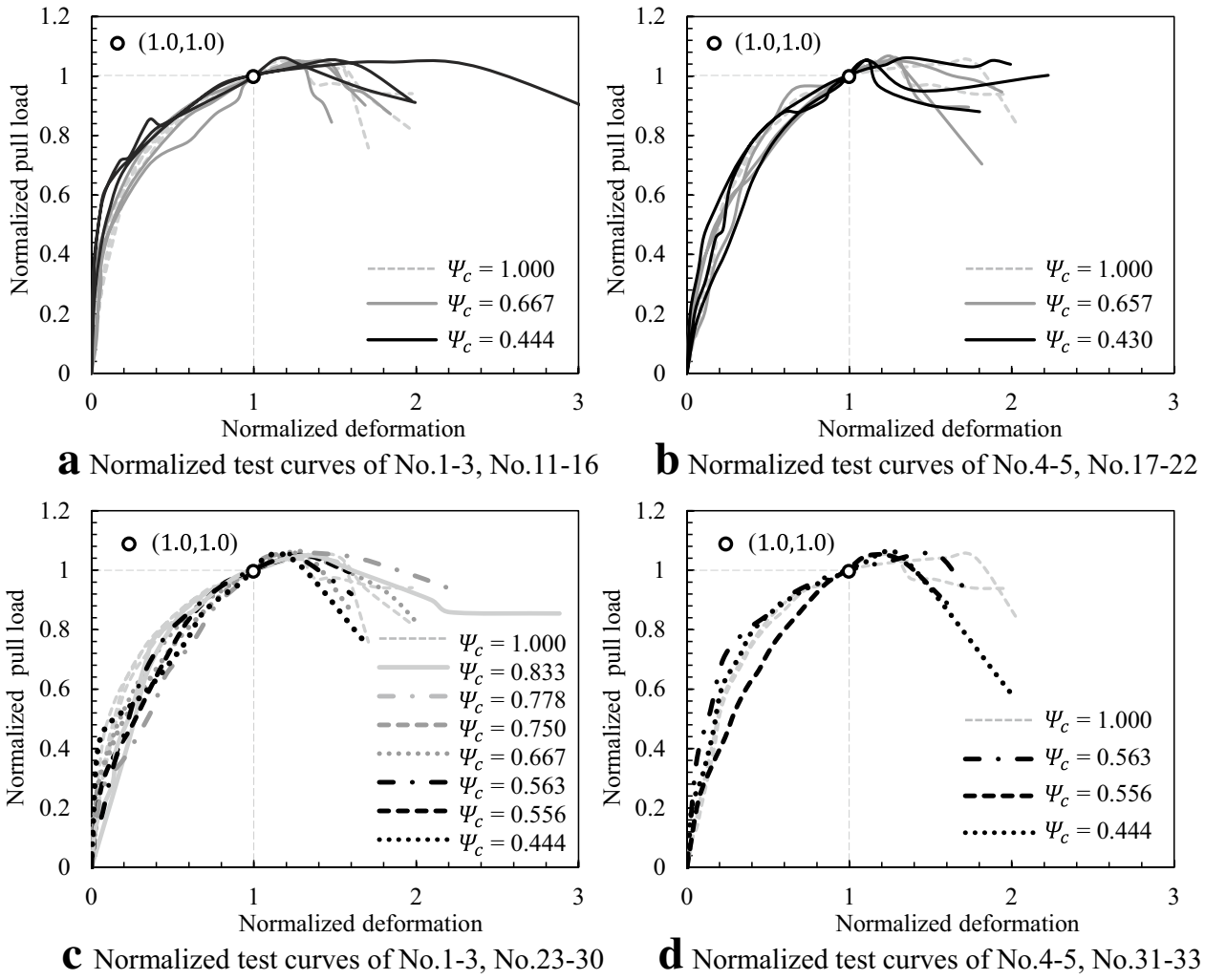

Fig. 13 Normalized load–deformation curves of the anchorage concrete with different boundaries.

peak bearing pressure is calculated by dividing the peak tensile force by the bearing area. It can be seen that, in the range of 300–800 MPa for the bearing pressure, the prediction modified by Eq. (4) seems more concentrated and accurate compared to the results at smaller bearing pressure. In general, prediction modified by Eq. (4) is applicable for a wide range of bearing pressure at stud head.

3.2 Determination of Critical Deformation δ_m

Based on the single-variable tests, the relationship between the increase ratio of the critical deformation and different design parameters is exhibited in Fig. 16. The research findings indicate that the increase of the concrete strength and bearing area can effectively reduce the critical deformation. However, the embedment depth and boundary effects (represented by Ψ_c) present the opposite effects. Furthermore, it can be observed that the exponential functions are the most appropriate model to fit the tendency of the relationships between the critical deformation and investigated design parameters, as indicated by the black dash line in Fig. 16.

In view of the trend line (the dash line) shown in Fig. 16, exponential functions are adopted in this paper to describe the relationships between the critical deformation and design parameters, as shown in Eq. (5). Here, Z_1 to Z_4 are the coefficients for assessing the sensitivity of the critical deformation to different parameters and Z_0 is the adjustment coefficient determined from the fitting curve of the collected test results.

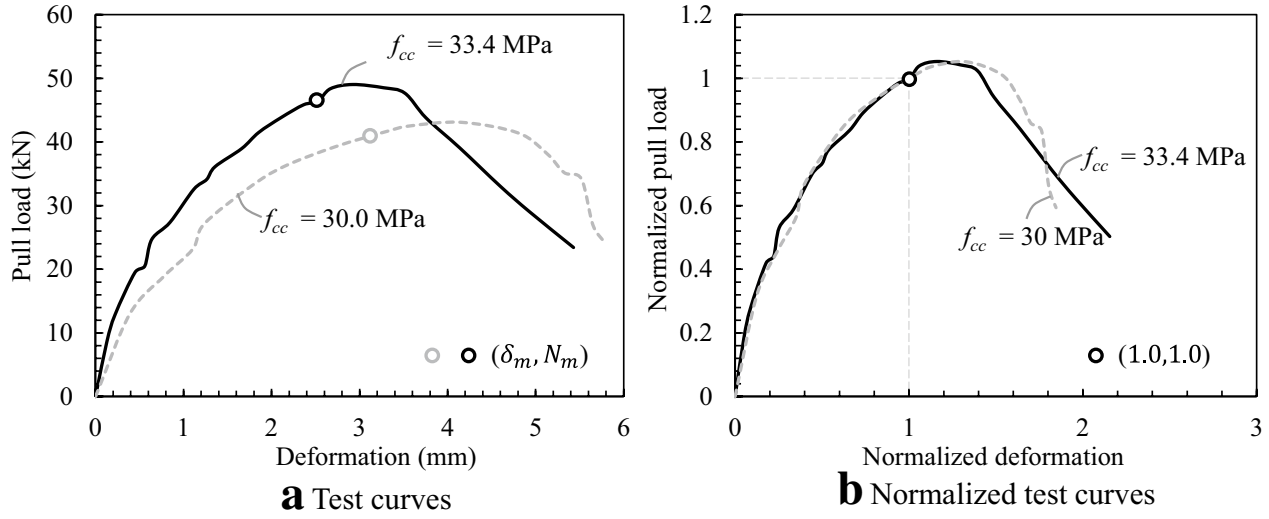

Fig. 14 Typical load–deformation curves of anchoring concrete with different concrete strengths.

Table 3 Design parameters of the collected load–deformation curves.

Source	Specimen number	h_{ef} (mm)	f_{cc} (MPa)	d_s (mm)	a (mm)	Ψ_c
Hanenkamp (1985)	2	195	27.3–31.3	22	6.5	0.80–1.00
Furche (1994)	4	80	33.4	12	3.0	1.00
Zhao (1991)	4	160	24.8–30.5	22	6.5	0.41–0.84
Bouska (1992)	14	150–450	28.3–34.4	24–72	4.45–31.5	1.00
Furche (1994)	5	80	30	12	0.5–4.0	1.00
Berger (2011)	8	160–180	26.9–27.6	22	6.5	0.49–1.00
Grand total	37	80–450	16.4–34.4	12–72	0.5–31.5	0.41–1.00

More detailed information about the test specimens is listed in Additional file 1: Appendix A. f_{cc} is the compressive strength of concrete cubes with side length of 200 mm; h_{ef} is the embedment depth of the headed stud; d_s is the diameters of the stud shank; a is the shoulder width of the stud head; Ψ_c is the boundary coefficient considering the influence of the free edges and group studs.

$$\delta_{\mathrm{m}} = e^{Z_0}\left(f_{cc}\right)^{Z_1}\left(h_{ef}\right)^{Z_2}(A_h)^{Z_3}(\Psi_c)^{Z_4} \tag{5}$$

After taking logarithm at both sides of Eq. (5), a linear function can be obtained as shown in Eq. (6), the units for f_{cc}, h_{ef} and A_h are, respectively, MPa, mm and mm^2. The $\ln(\delta_m)$ is treated as the response variable. The $\ln(f_{cc})$, $\ln(h_{ef})$, $\ln(A_h)$, and $\ln(\Psi_c)$ are employed as the explanatory variables.

$$\begin{aligned}\ln(\delta_{\mathrm{m}}) &= Z_0 + Z_1\ln(f_{cc}) + Z_2\ln(h_{ef}) + Z_3\ln(A_h) + Z_4\ln(\Psi_c)\\ &= -2.84 - 0.86\ln(f_{cc}) + 2.66\ln(h_{ef}) - 1.04\ln(A_h) + 2.59\ln(\Psi_c)\end{aligned} \tag{6}$$

A multiple linear regression analysis on the collected test results is performed to predict $\ln(\delta_m)$ from the $\ln(f_{cc})$, $\ln(h_{ef})$, $\ln(A_h)$ and $\ln(\Psi_c)$. As summarized in Table 4, the multiple correlation coefficient (R) is up to 0.97 and the p value of the significance (F) is nearly to zero, indicating that the model can efficiently predict the relationship between the response and explanatory variables. The p value corresponding to each regression coefficient is much smaller than 0.05, which demonstrates that the critical deformation is significantly dependent on the investigated design parameters.

The comparison between measured and predicted critical deformations is displayed in Fig. 17. The average (AVE) and standard deviation (STD) of the ratio between test data and prediction results are 1.04 and 0.31, respectively. A moderate dispersion of the prediction results can be found due to the complicated influence of many factors. In fact, the critical deformation of the anchorage

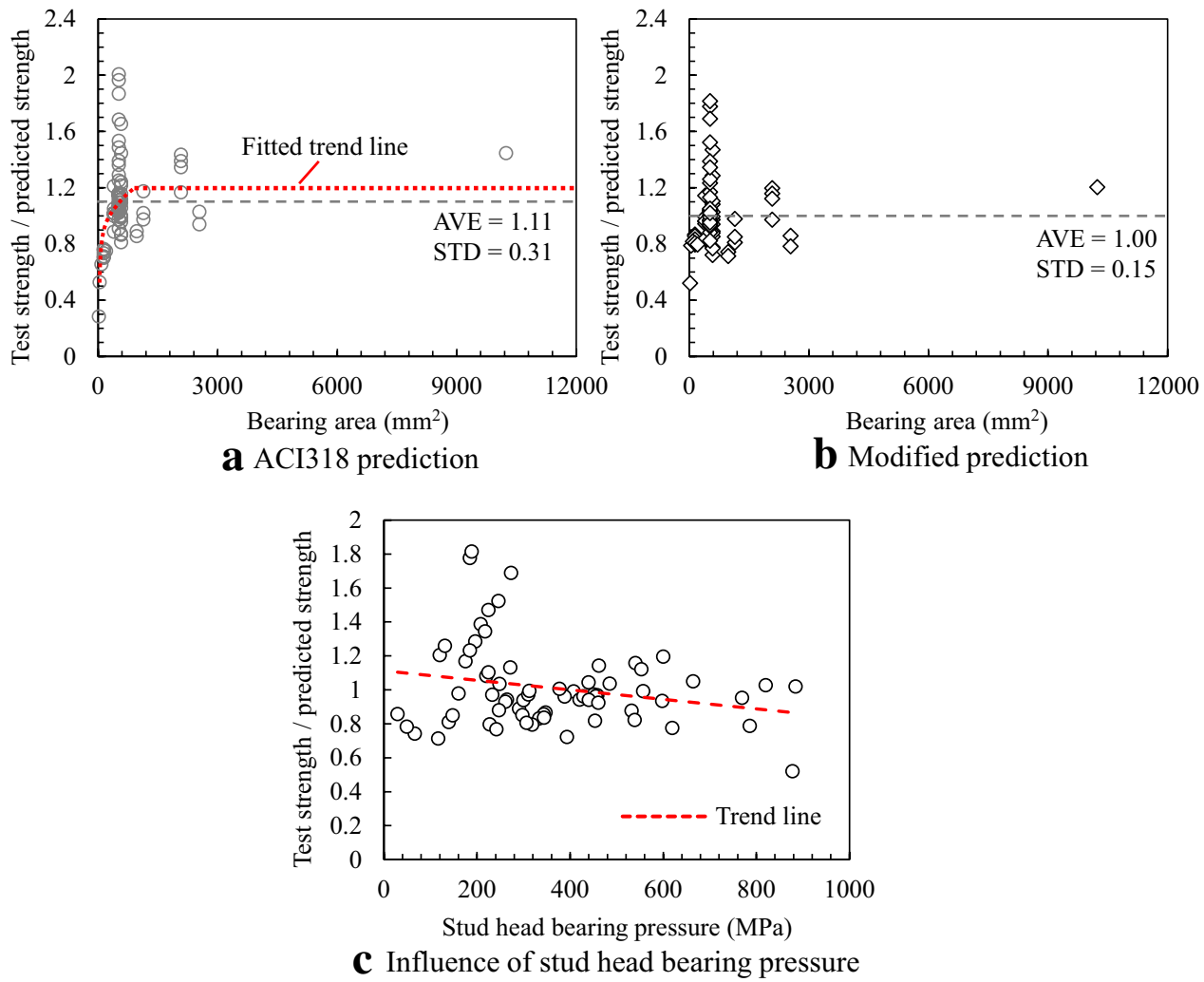

Fig. 15 Influence of bearing area on the concrete anchorage capacity.

concrete is influenced by many accidental factors (Berger, 2015) in actual practice, including the cracking of the breakout surface, the concrete aggregate size and even concrete casting direction, which can hardly be considered in this study. For example, in the pullout tests conducted by Furche (1986), specimen U390Vo3 and U390Vo4 (as shown in Additional file 1: Table S1 of Appendix A) have identical design parameters while their critical deformation are, respectively, 2.52 mm and 1.58 mm, with a much larger STD than 0.31. Therefore, from the perspectives of design, the STD value of 0.31 is acceptable when predicting the critical deformation of the anchorage concrete, and Eq. (5) is practicable and feasible.

3.3 Determination of Mathematical Expression for Normalized Load–Deformation Curves

In Sect. 2.4, it has been demonstrated that the design parameters have much less influence on the normalized load–deformation curves compared with the critical load or critical deformation, especially for the ascending branches. Therefore, a piecewise function with three segments corresponding to three loading stages is adopted to fit the normalized curves, as shown by the red dotted line in Fig. 18.

In the ascending stage, the relationship between the normalized load [N] and normalized deformation [δ] can be described as Eq. (7). By adjusting the specific value of the coefficients denoted as m and n, different ascending patterns can be obtained to fit the stiffness degradation

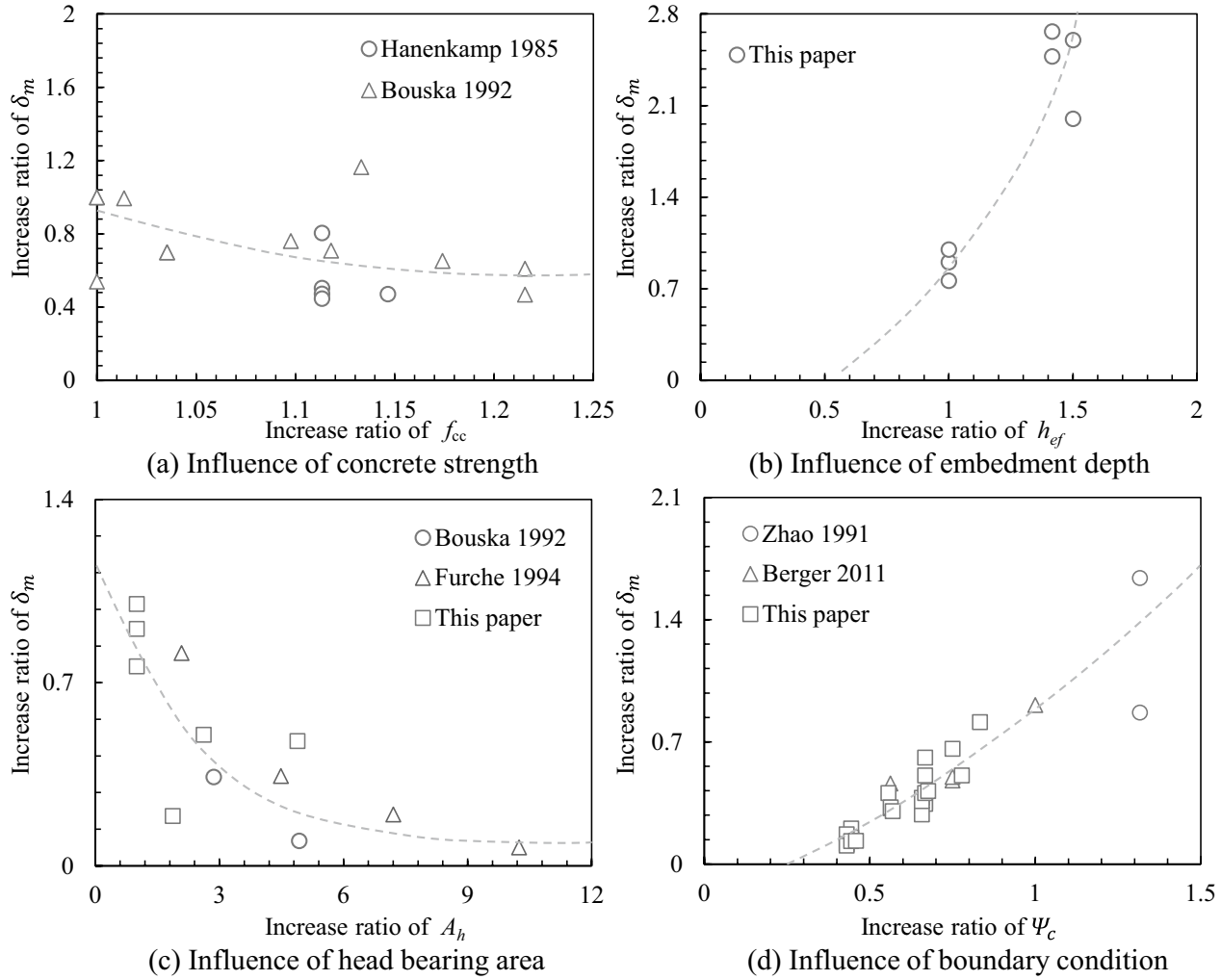

Fig. 16 Influence of different factors on the increase of critical deformation.

Table 4 Results of the multiple linear regression analysis.

Correlation coefficient *R*	*p* value of significance (*F*)		Regression coefficient	Standard error	Statistic t	*p*
0.97	0.000	Intercept	− 2.84	1.00	− 2.831	0.006
		$ln(f_{cc})$	− 0.86	0.22	− 3.924	0.000
		$ln(h_{ef})$	2.66	0.13	20.091	0.000
		$ln(A_h)$	− 1.04	0.06	− 17.265	0.000
		$ln(\Psi_c)$	2.59	0.12	21.262	0.000

R, *F*, t and *p* are statistical values describing the results of the multiple linear regression analysis. f_{cc} is the compressive strength of concrete cubes with side length of 200 mm; h_{ef} is the embedment depth of the headed stud; A_h is the bearing area of stud head; Ψ_c is the boundary coefficient considering the influence of the free edges and group studs.

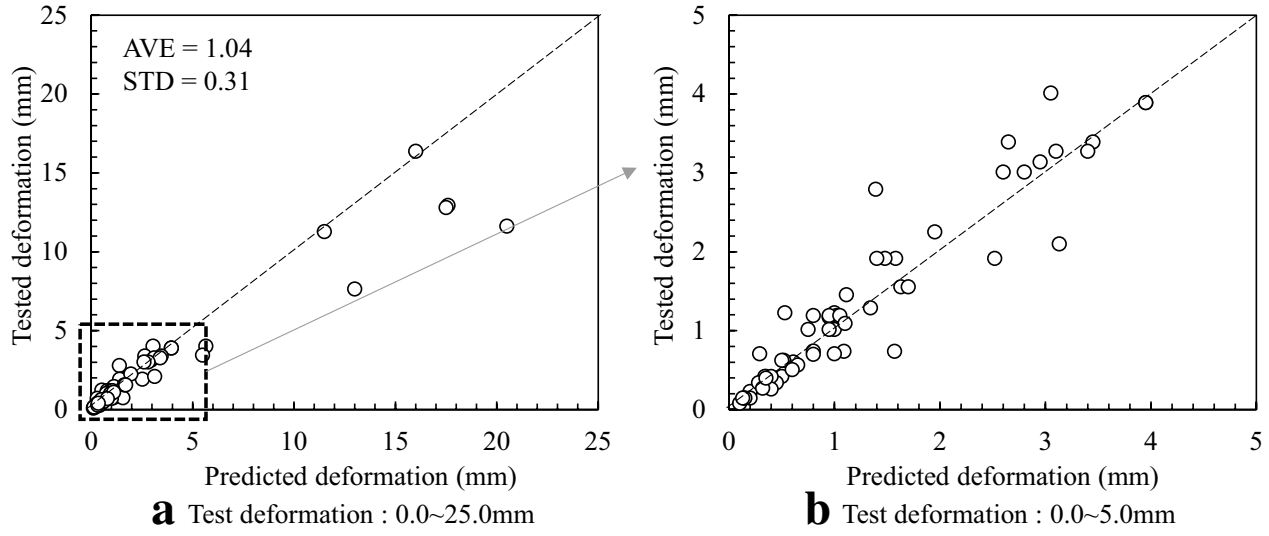

Fig. 17 Comparison between test data and prediction results of the critical deformation.

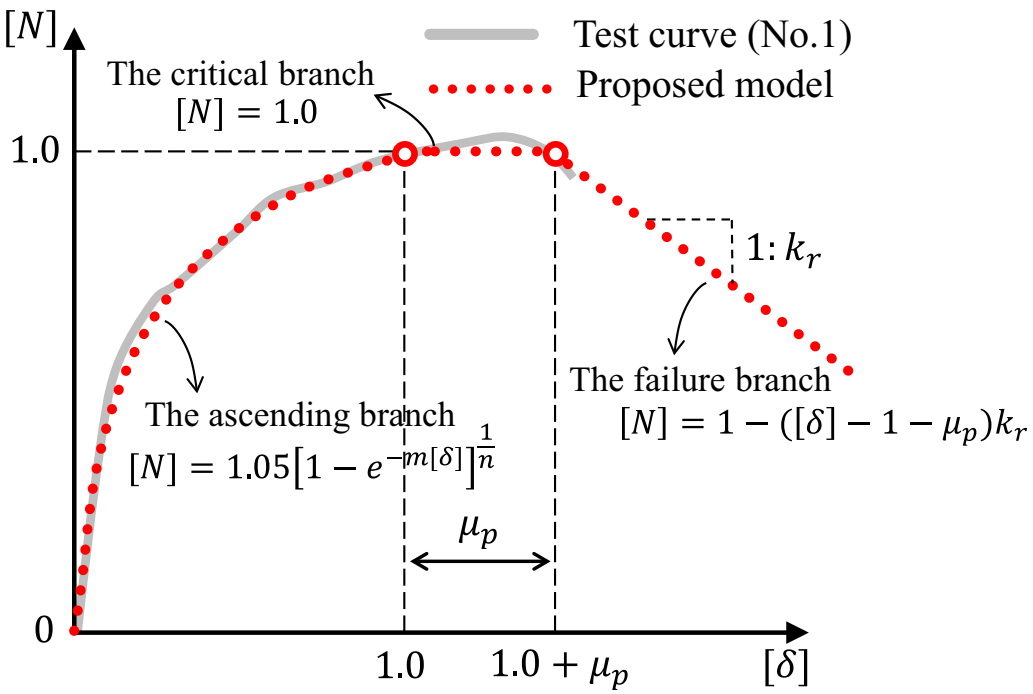

Fig. 18 Mathematical expression of the normalized load–deformation curves.

features of the normalized curves of the anchorage concrete.

$$[N] = 1.05(1 - e^{-m[\delta]})^{\frac{1}{n}} \tag{7}$$

To determine m and n in Eq. (7), two constraint conditions are needed, as shown in Eqs. (8) and (9). In Eq. (9), A_w stands for the area between the normalized curves and the horizontal axis in the ascending stage. Equation (8) guarantees that the critical point is located at the characteristic point (1.0, 1.0) in the normalized coordinate system, and Eq. (9) ensures that Eq. (7) is accurate from the perspective of energy dissipation.

$$1.00{=}1.05(1 - e^{-m})^{\frac{1}{n}} \rightarrow m = -\ln(1 - 0.95^n) \tag{8}$$

$$\int_0^1 1.05(1-e^{-m[\delta]})^{\frac{1}{n}} d[\delta] = A_w \tag{9}$$

Combined with Eqs. (8) and (9), the value of n can be uniquely determined according to the value of A_w, as expressed in Eq. (10).

$$\int_0^1 1.05[1-(1-0.95^n)^{[\delta]}]^{\frac{1}{n}} d[\delta] = A_w \tag{10}$$

In the critical stage, the remarkable deformation increment is induced by the rapid and unstable propagation of the cracks of the breakout concrete. However, the strength increment of the anchorage concrete is still limited, which is in good agreement with the conclusions in above sections. Therefore, the constant function $[N]=1.0$ is conservatively adopted in the stage before reaching the failure point. To evaluate the deformation capacity of the anchorage concrete in the critical stage, the ductility coefficient (μ_p) is defined as the length between the critical and failure point in the normalized curves. Therefore, the deformation at the failure point (referred as the failure deformation, δ_u) can be further obtained according to Eq. (11).

$$\delta_u = (1+\mu_p)\delta_m \tag{11}$$

After the failure point, a steep descending branch in the normalized load–deformation curves is observed because of the breakout of the anchorage concrete, especially for the single stud without sufficient constraints provided by the surface reinforcement. According to the discussion on typical normalized pullout curves, the descending branches varies obviously and irregularly. For simplification, the failure stage is represented by a linear function starting from the failure point and drops with the maximum secant stiffness (referred as the residual stiffness k_r) in the failure stage. Conclusively, the normalized pullout curves of the anchorage concrete can be given by Eq. (12).

$$[N] = \begin{cases} 1.05[1-(1-0.95^n)^{[\delta]}]^{\frac{1}{n}} & [\delta] < 1.00 \\ 1.00 & 1.00 \le [\delta] < 1.00+\mu_p \\ 1.00-([\delta]-1-\mu_p)k_r & [\delta] \ge 1.00 \end{cases} \tag{12}$$

Based on the collected pullout curves, the variation and distribution of the coefficients n, μ_p and k_r in Eq. (12) are presented in Fig. 19a–c. Compared with the coefficients corresponding to the critical and failure branches, the degree of discretization for the coefficient n in the ascending branch is relatively smaller, ranging from 0.3 to 2.4. For comparison, the function image of the Eq. (12) and all normalized curves of the collected experimental data are summarized in Fig. 19d. It can be concluded that, when n, μ_p and k_r take their average values, respectively, the proposed equation can appropriately predict the evolution of the normalized load–deformation curves.

4 Verification of Proposed Analytical Model

Considering the average values of the coefficients in Eq. (12), the mathematical expression of the proposed analytical model can be further described as Eq. (13), where N_u, Ψ_h, and δ_m are determined by Eqs. (3), (4) and (6), respectively.

$$N_m = N_m(\delta)\begin{cases} \psi_h N_u[1-0.05^{\frac{\delta}{\delta_m}}]^{1.02} & \delta < \delta_m \\ 0.95\psi_h N_u & \delta_m \le \delta < 1.48\delta_m \\ 0.48\psi_h N_u(3.48-\frac{\delta}{\delta_m}) & \delta \ge 1.48\delta_m \end{cases} \tag{13}$$

In the following sections, the effectiveness of the proposed model will be verified through the comparison between experimental observations from typical pullout tests of headed studs and semi-rigid joint tests and the predicted results using the Eq. (13) proposed in this study.

4.1 Verification with Typical Pullout Tests

The comparison between the predicted curves and all available experimental data is summarized in Additional file 1: Appendix B. The typical load–deformation curves with different design parameters are presented in Fig. 20. It can be clearly seen that the load–deformation behavior of the anchorage concrete with different bearing areas, embedment depths, boundary conditions can be accurately predicted using the proposed model.

Figure 21 shows the ratios of the measured deformation to the predicted deformation corresponding to the loading levels of 30%N_u, 60%N_u and 90%N_u, respectively. As illustrated in the figure, the average values are 0.89, 1.08 and 1.20, indicating that the proposed model can well estimate the deformation capacity of the anchorage concrete under different tension states.

4.2 Verification with Typical Semi-rigid Joint Tests

In general, the failure of typical semi-rigid joints is dominated by the breakout of anchorage concrete. In this section, the rotational behavior of the column–base joint anchored by headed studs (Rybinski, 2014) is investigated by considering the deformation of the anchorage concrete, as shown in Fig. 22a. According to the component method recommended by EC3 Part 1–8 (2004), the tension force (F_T) induced by the bending moment (M) of the column is sequentially transmitted to the base through the T-stub, stud shank and anchorage concrete.

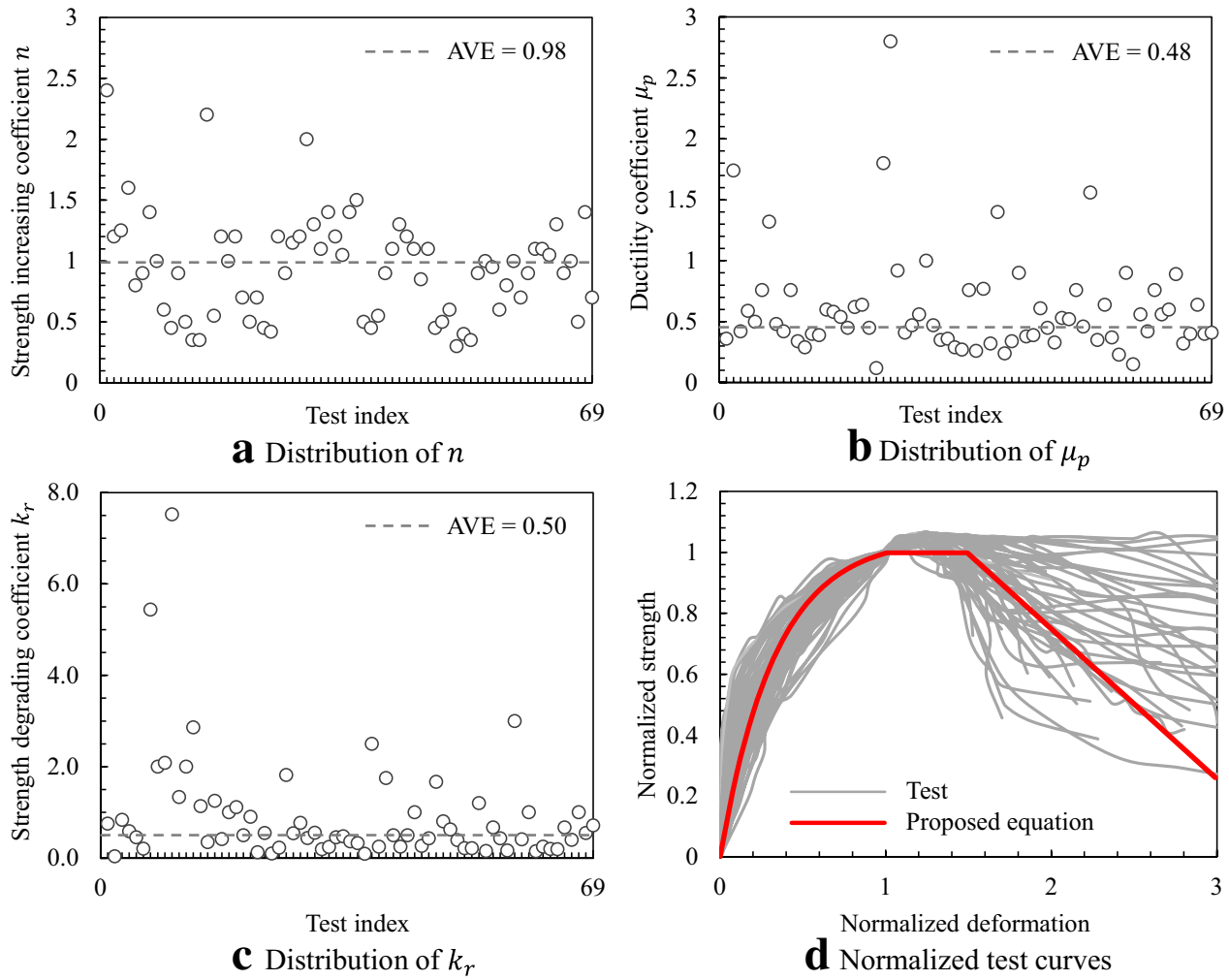

Fig. 19 Determination of the coefficients in Eq. (12).

Meanwhile, the compression force (F_C) can directly transfer to the concrete surface through the end plate contacted to the top surface of the anchorage concrete. Therefore, the rotational behavior of the column–base is primarily determined by the aforementioned four displacement components which are represented by $\triangle_{stub}$, $\triangle_{shank}$, $\triangle_{t\text{-}con}$ and $\triangle_{c\text{-}con}$, respectively, as illustrated in Fig. 22b.

According to moment equilibrium of the joint, F_T and F_C can be obtained according to Equation (14).

$$F_T = F_C = \frac{M}{L_M} \tag{14}$$

The rotation of the column–base joint R can be defined as Eq. (15).

$$R = \frac{\Delta_{stub} + \Delta_{shank} + \Delta_{t-con} + \Delta_{c-con}}{L_M} \tag{15}$$

Before the yielding of the stud shank or crushing of the concrete at the compression side, $\triangle_{stub}$, $\triangle_{shank}$, and $\triangle_{c\text{-}con}$ are proportional to F_T or F_C, respectively. Therefore, the contribution of these three components can be represented by an equivalent spring component whose deformation ($\triangle_{eq}$) and stiffness (K_{eq}) are defined by Eqs. (16) and (17). Here, K_{stub}, K_{shank} and $K_{c\text{-}con}$ represent the elastic stiffness of the corresponding components according to EC3 Part 1–8.

$$\begin{aligned}\Delta_{eq} &= \Delta_{stub} + \Delta_{shank} + \Delta_{c-con} \\ &= \frac{F_T}{K_{stub}} + \frac{F_T}{K_{shank}} + \frac{F_C}{K_{c-con}} = \frac{F_T}{K_{eq}}\end{aligned} \tag{16}$$

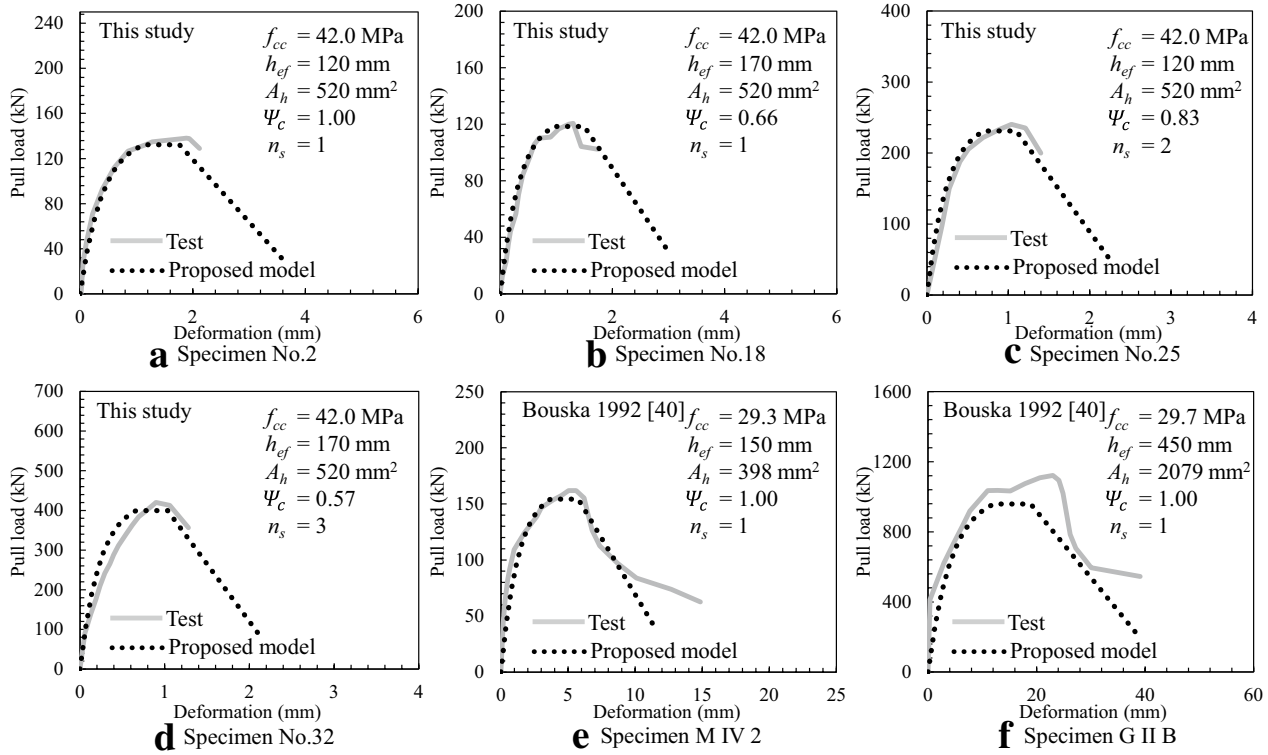

Fig. 20 Comparison of typical test curves and the proposed model.

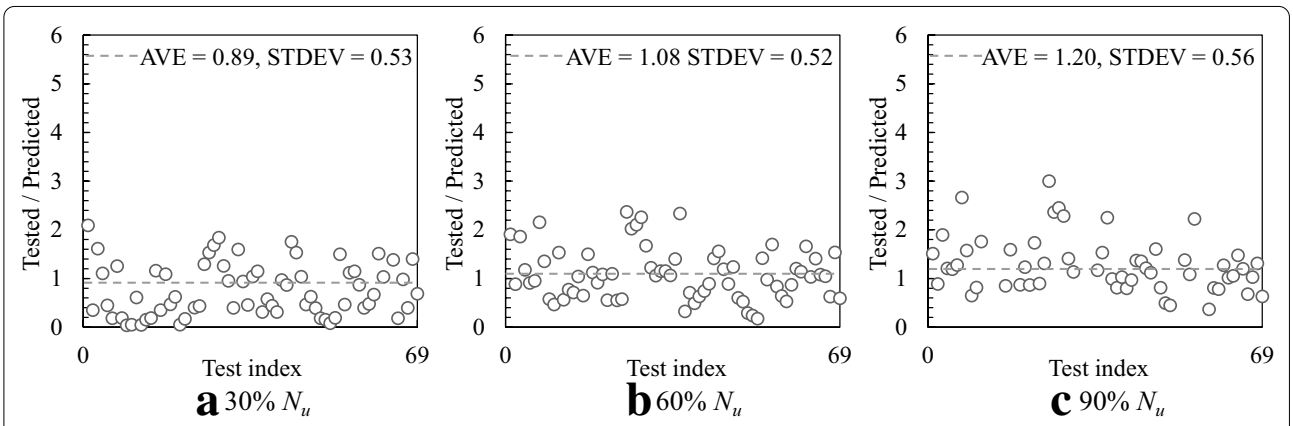

Fig. 21 Overall comparison between the tests and the proposed model.

$$\frac{1}{K_{eq}} = \frac{1}{K_{stub}} + \frac{1}{K_{shank}} + \frac{1}{K_{c-con}} \tag{17}$$

Referencing to Eqs. (14)–(17), R and M can be represented as functions of $\triangle_{t\text{-}con}$ (respectively, referred as R($\triangle_{t\text{-}con}$) and M($\triangle_{t\text{-}con}$)), as expressed in Eqs. (18) and (19), where $N(\triangle_{t\text{-}con})$ denotes the reaction force of the anchorage concrete determined according to Equation (13).

$$M = M(\Delta_{t-con}) = F_T L_M = N(\Delta_{t-con}) L_M \tag{18}$$

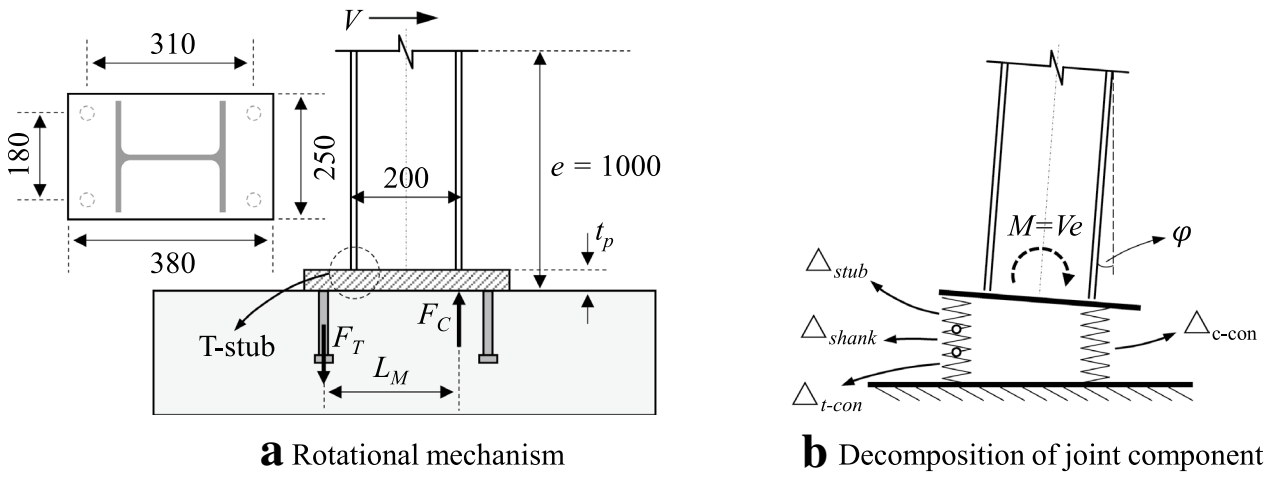

Fig. 22 Load transferring mechanism of semi-rigid joint and deformation decomposition.

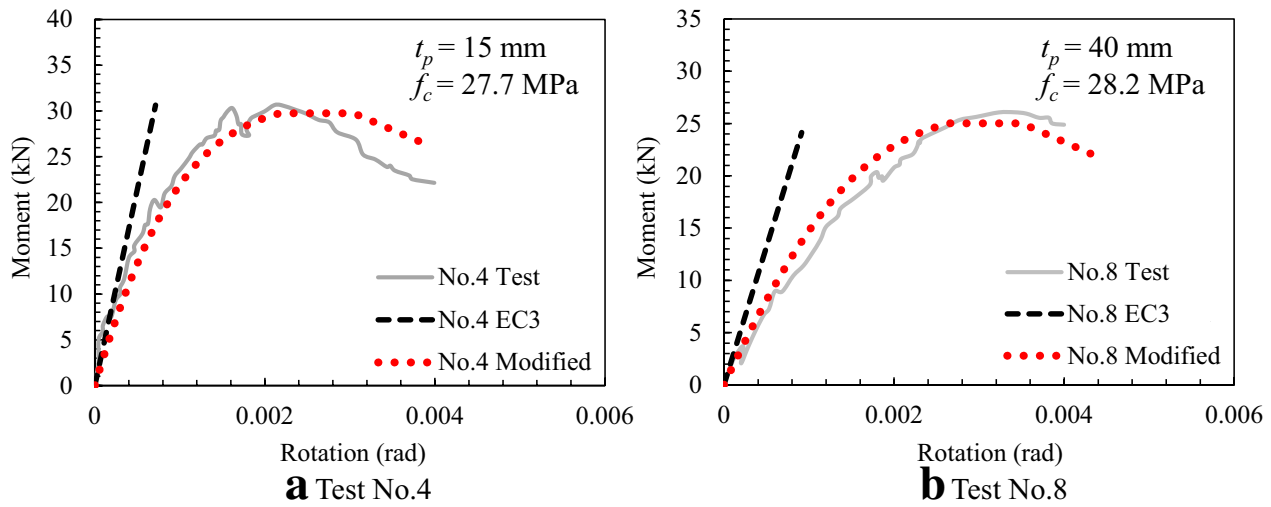

Fig. 23 Moment–rotation curves of typical semi-rigid joints.

$$R = R(\Delta_{t-con}) = \frac{\Delta_{t-con} + \Delta_{eq}}{L_M} = \frac{\Delta_{t-con} + F_T/K_{eq}}{L_M} = \frac{\Delta_{t-con} + N(\Delta_{t-con})/K_{eq}}{L_M} \tag{19}$$

The moment–rotation (M–R) curves of the column–base joint with different design parameters are shown in Fig. 23. The M–R curves according to EC3, which ignores the contribution of the anchorage concrete by assuming $\triangle_{t\text{-}con} = 0$ are also plotted for comparison. It is noticeable that the rotational behavior of the column–base joint including the gradual degradation of stiffness, rapid growth of rotation during concrete breakout and the decrease of strength can be well predicted while considering the deformation of the anchorage concrete in the proposed analytical model. On the contrary, ignoring the influence of the anchorage concrete will significantly underestimate the joint deformation.

To further evaluate the influence of the anchorage concrete before reaching structural failure of the joints, the ratio of rotation (R_{ac}) induced by the anchorage concrete in the total rotation of the joint is defined in Eq. (20), where F_T is taken as the minimal tensile resistance between the T-stub (N_T), stud shank (N_s) and anchorage

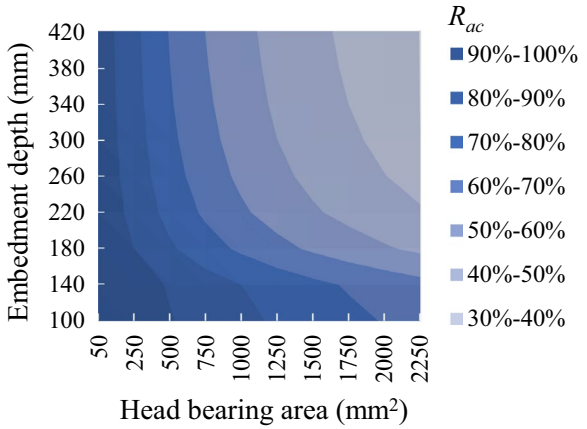

Fig. 24 Contribution of the anchorage concrete to the rotation of the column–base joint.

concrete (N_m). The specific value of N_T and Ns can be determined according to EC3 Part 1–8.

$$R_{ac} = \frac{\Delta_{t-con}}{\Delta_{t-con} + \Delta_{eq}} = \ln[1 - (\frac{F_T}{\Psi_h N_u})^{0.98}]/(\ln[1 - (\frac{F_T}{\Psi_h N_u})^{0.98}] + \frac{3F_T}{\delta_m K_{eq}}) \quad (20)$$

Figure 24 shows the distribution of R_{ac} of the investigated column–base joints with different stud bearing areas and embedment depths. Here, the thickness of the endplate (t_p) and compressive strength (f_c) of the anchorage concrete are set to 40 mm and 30 MPa, respectively. For anchorage concrete with small bearing area and shallow embedment, the contribution of the anchorage concrete in the rotation of the joint is dominant. Despite the fact the increment of the bearing area and embedment depth will lower the value of R_{ac}, the influence of the anchorage concrete exceeds 30% of the joint rotation, indicating that the contribution of the anchorage concrete should be considered in practical applications.

5 Conclusions

Experimental study on a total of 33 pullout test specimens is conducted to investigate the whole-process tensile behavior of the anchorage concrete. To quantitatively determine the influence of embedment depth, bearing area, boundary conditions and concrete strength on the load-bearing capacity and the characteristic of load–deformation curves of the anchorage concrete, a total of 37 test results from currently reported literatures are additionally collected for parametric analysis. A new analytical model represented by a piecewise function is proposed to describe the whole-process load–deformation behavior of the anchorage concrete and applied to simulate the rotational behavior of the typical semi-rigid joint anchored by headed studs. The major conclusions can be drawn as follows:

(1) The prevalent concrete capacity design (CCD) method specified by ACI318-14 can effectively predict the capacity of the anchorage concrete with different design parameters including embedment depth, boundary conditions, and concrete strength. A modification factor is further proposed to improve the prediction accuracy of the CCD methods, which can properly evaluate the influence of the bearing area on concrete capacity.
(2) The deformation capability of the anchorage concrete significantly depends on the embedment depth, bearing area of stud head, boundary conditions and concrete strength, which can be well described by a proposed exponential function. The efficiency of the proposed exponential function is verified by the test data and the analytical results matches well with the test data.
(3) Typical pullout process of the anchorage concrete can be segmented into three stages: the ascending stage, critical stage, and failure stage. The load–deformation relationships of different stages can be depicted by exponential function, constant function, and linear function, respectively. The proposed piecewise function composed of these three functions corresponding to each pullout stage can assess accurately the load–deformation behavior of the anchorage concrete with different design parameters.
(4) The rotational behavior of typical semi-rigid joints can be accurately predicted using the proposed analytical model which considers the contribution of the anchorage concrete. The influence of the anchorage concrete plays a dominant role in the rotational behavior of semi-rigid joint anchored by headed studs, which should be paid enough attention to in practical engineering applications.

It is worth noting that in most cases, the headed studs are pulled with the combination of shear force, and the shear force may have strong influence on the pull-out capacity and deformability. Therefore, it is proposed to conduct further research on the behavior of headed studs under combined shear and tensile loads.

Abbreviations

a: Shoulder width of the stud head; A_d: Cross-sectional area of the stud shank; A_h: Bearing area of the stud head (mm^2); A_{Nc}: Actual projected failure area of the breakout concrete cone; A_{Nco}: Total projected failure area the breakout concrete cone; A_w: Enclosed area of the ascending segment of the normalized load–deformation curves; C_a: Edge distance of the stud; E_s: Young's modulus of the headed stud steel; f_{cc}: Compressive strength of the concrete cubes with side length of 200 mm (MPa); f_{yk}: Yielding strength of steel reinforcement; h_{ef}: Embedment depth of the headed stud (mm); K_i: Stiffness of the ith component of the column–base joint; K_{eq}: Stiffness of the equivalent component of the column–base joint; L_M: Distance between tensile and compressive resultant force of the column–base joint; m, n, k_r, μ_p: Coefficients of the piecewise function describing the normalized load–deformation curve; M, F_T, F_C: Internal forces of the column–base joint; n_s: Number of headed studs; N_u: Ultimate strength of the anchorage concrete; N_m: Critical strength of the anchorage concrete; R, F, t, p: Statistical values describing the results of the multiple linear regression analysis; R_{ac}: Ratio of rotation induced by the anchorage concrete to the total joint rotation; S: Spacing of group studs; t_p: Thickness of the endplate of the column–base joint; P: Applied tensile load of the headed stud; Z_0—Z_4: Coefficients in the equation determining the critical deformation of the anchorage concrete; μ_p: Ductility coefficient determining the length of the critical stage of the normalized load–deformation curve; Ψ_c: Boundary coefficient considering the influence of the free edges and group stud; $\Psi_{ed,N}$: Modification factor considering the influence of asymmetric stress distribution in the presence of free edges; Ψ_h: Modification factor considering the influence of bearing area of the stud head; δ_u: Ultimate deformation of the anchorage concrete; δ_m: Critical deformation of the anchorage concrete; [M]: Normalized strength; [δ]: Normalized deformation; $\triangle_i$: Displacement of the ith component of the column–base joint; $\triangle_{eq}$: Displacement of the equivalent component of the column–base joint.

Supplementary Information

The online version contains supplementary material available at https://doi.org/10.1186/s40069-021-00464-x.

Additional file 1: Table S1. Collection of Headed Stud Pullout Tests (Unit: N, mm). **Figure S1.** Comparison between test curves and predicted curves.

Acknowledgements

The authors gratefully acknowledge the financial support provided by the National Natural Science Foundation of China (Grant No. 51890903).

Authors' contributions

Y. M. conducted the experiment and collected the data; L. Z. processed the data and proposed the analytical model, and draft this manuscript; H. C. checked the proposed model and writing. R. D. initiated and supervised the whole research. All authors read and approved the final manuscript.

Authors' information

LZ and YM are graduate students at Tsinghua University; HC is a post-doctoral researcher at Tsinghua University; and RD is an assistant professor at Tsinghua University.

Funding

National Natural Science Foundation of China (Grant No. 51890903).

Availability of data and materials

The experimental data used to support the observations of this study are included in the article.

Declaration

Competing interests

The authors declare that they have no competing interests.

Author details

[1]Key Lab. of Civil Engineering Safety and Durability of China Education Ministry, Dept. of Civil Engineering, Tsinghua University, Beijing 100084, China. [2]Beijing Engineering Research Center of Steel and Concrete Composite Structures, Tsinghua University, Beijing 100084, China.

Received: 8 October 2020 Accepted: 13 April 2021
Published online: 19 May 2021

References

American Concrete Institute Committee 349 (ACI). (2006). Code requirements for nuclear safety related concrete structures (ACI 349–06). Farmington Hills (MI): American Concrete Institute.

American Concrete Institute Committee 318 (ACI). (2014). Building code requirements for structural concrete (ACI 318–14) and commentary (ACI 318R-14). Farmington Hills (MI): American Concrete Institute.

Berger, W. (2011). Zug- und Querlastversuche an Kopfbolzen und Verbunddübeln mit und ohne Rückhängebewehrung – Versuchsbericht (Tensile and shear load tests on head studs and bonded anchors with and without back-up reinforcement - test report). Bericht-Nr. fHW/22–11/06, Institut für Werkstoffe im Bauwesen, Universität Stuttgart.

Berger, W. (2015). Trag- und Verschiebungsverhalten sowie Bemessung von Kopfbolzenverankerungen mit und ohne Rückhängebewehrung unter Zuglast (Load and displacement behavior as well as dimensioning of head bolt anchorages with and without back-up reinforcement under tensile load). Dissertation, Universität Stuttgart.

Bouska, P. (1992). *Analysis of experimental data of the pull-out tests of anchor bolts*. Czech Technical University in Prague.

Chang, X., Chen, H., Liu, B., & Zhao, F. (2011). Modeling of anchor bolt pullout in concrete based on a heterogeneous assumption. *Nuclear Engineering and Design, 241*(5), 1345–1351

CMC. (2010). *Code for design of concrete structures. GB50017–2010*. Beijing, China Ministry of Construction.

Derek, P., Lin, Z. B., Zhao, & J. (2013). *Behavior and design of cast-in-place anchors under simulated seismic loading—NEES-anchor project, final report*. National Science Foundation for the NEESR Project.

Eligehausen, R., Mallée, R., & Silva, J. F. (2006). *Anchorage in Concrete Construction*, First edition. Ernst & Sohn: Berlin, Germany.

Eligehausen, R., Werner, F., & Sippel, T. M. (1998). Anchorage to concrete. *Progress in Structural Engineering & Materials, 1*(4), 392–403

EN 1993-1-8. (2004). *Eurocode 3: design of steel structures. Part 1–8: Design of joints*. Brussels: Comité Européen de Normalisation (CEN) 2004.

Fuchs, W. (1995). Concrete capacity design (CCD) approach for fastening to concrete. *ACI Structural Journal, 92*, 73–94

Furche, J. (1994). *Zum Trag- und Verschiebungsverhalten von Kopfbolzen bei zentrischem Zug (For the carrying and shifting behavior of head bolts in centric tension)*. Dissertation, Universität Stuttgart.

Furche, J., & Dieterle, H. (1986). *Ausziehversuche an Kopfbolzen mit unterschiedlichen Kopfformen bei Verankerungen im ungerissenen Beton und in Parallelrissen (Pull-out tests on head bolts with different head shapes for anchorages in non-cracked concrete and in parallel cracks)*. Bericht Nr. 9/1–86/9, Institut für Werkstoffe im Bauwesen, Universität Stuttgart.

Grauvilardell, J., Lee, D., Hajjar, J.F., & Dexter, R. (2005). *Synthesis of design, testing and analysis research on steel column base plate connections in high-seismic zones*. Structural Engineering Report No. ST-04–02, Minneapolis, MN, University of Minnesota.

Hanenkamp, W., Wunderlich, W. (1985). *Tragverhalten von Verankerungen mit Kopfbolzen. Zusatzversuche Serie 4 und 5 (Structural behavior of anchorages with headed bolts. Additional tests of Series 4 and 5)*. Zugtragfähigkeit von EinzelKopfbolzen mit unterschiedlichen Randabständen (Capaity of single headed studs with different edges). Bericht Nr. A-04/85-4/5-1, Institut für Konstruktiven Ingenieurbau, Ruhr-Universität Bochum.

Henriques, J., Raposo, J. M., Da Silva, L. S., & Neves, L. C. (2013). Tensile resistance of steel-reinforced anchorages: Experimental evaluation. *ACI Structural Journal, 110*(2), 239–250

Hoehler, M., & Eligehausen, R. (2008). Behavior and testing of anchors in simulated seismic cracks. *ACI Structural Journal, 105*(3), 348–357

Latour, M., Piluso, V., & Rizzano, G. (2014). Rotational behaviour of column base plate connections: Experimental analysis and modelling. *Engineering Structures, 68*, 14–23

Latour, M., & Rizzano, G. (2019). Mechanical modelling of exposed column base plate joints under cyclic loads. *Journal of Constructional Steel Research, 162*, 105726

Lee, N. H., Kang, S. K., Chang, J. B., & Park, K. R. (2007). Tensile-headed anchors with large diameter and deep embedment in concrete. *ACI Structural Journal, 104*(4), 479–486

Nilforoush, R., ASCE SM, Nilsson, M., & Elfgren, L. (2018). Experimental evaluation of influence of member thickness, anchor-head size, and orthogonal surface reinforcement on the tensile capacity of headed anchors in uncracked concrete. *Journal of the Structural Engineering. American Society of Civil Engineers, 144*(4), 04018012

Nilforoush, R., Nilsson, M., Elfgren, L., Ozbolt, J., Hofmann, J., & Eligehausen, R. (2017a). Influence of surface reinforcement, member thickness, and cracked concrete on tensile capacity of anchor bolts. *ACI Structural Journal, 114*(6), 1543–1556

Nilforoush, R., Nilsson, M., Elfgren, L., Ozbolt, J., Hofmann, J., & Eligehausen, R. (2017b). Tensile capacity of anchor bolts in uncracked concrete: influence of member thickness and anchor's head size. *ACI Structural Journal, 114*(6), 1519–1530

Ottosen, N. S. (1981). Nonlinear finite element analysis of pull-out test. *ASCE, Journal of the Structural Division, 107*(4), 591–603

Ozbolt, J., & Eligehausen, R. (1993). *Fastening elements in concrete structures—numerical simulations*. Fracture and damage of concrete and rock, pp. 527–547

Ozbolt, J., Eligehausen, R., & Goran, P. (2003). *3D FE Analysis of anchor bolts with large embedment depths*. Symposium on Computing in Engineering.

Ozbolt, J., Eligehausen, R., & Reinhardt, H. W. (1999). Size effect on the concrete cone pull-out load. *International Journal of Fracture, 95*(1), 391–404

Pallarés, L., & Hajjar, J. F. (2010). Headed steel stud anchors in composite structures, Part II: Tension and interaction. *Journal of Constructional Steel Research, 66*(2), 213–228

Piccinin, R., Ballarini, R., & Cattaneo, S. (2010). Linear elastic fracture mechanics pullout analyses of headed anchors in stressed concrete. *Journal of Engineering Mechanics, 136*(6), 761–768

Prestressed Concrete Institute (PCI). (2004). *PCI design handbook*. (6th ed.). Precast/Prestressed Concrete Institute.

Rybinski, M. (2014). *Komponentenmethode für Ankerplatten mit Kopfbolzen unter einachsiger Beanspruchung (Component method for anchor plates with headed bolts under uniaxial loading)*. Dissertation, Institut für Konstruktion und Entwurf der Universität Stuttgart.

Shahrooz, B. M., Deason, J. T., & Tunc, G. (2004). Outrigger beam-wall connections. I: Component testing and development of design model. *Journal of Structural Engineering, 130*(2), 253–261

Tsavdaridis, K. D., Shaheen, M., Baniotopoulos, C., & Salem, E. (2016). Analytical approach of anchor rod stiffness and steel base-plate calculation under tension. *Structures, 5*, 207–218

Wald, F., Sokil, Z., & Jaspart, J. P. (2008). Base plate in bending and anchor bolts in tension. *Heron, 53*(1–2), 21–50

Wang, J., Navi, P., & Huet, C. (1993). *Finite element analysis of anchor bolt pull-out based on fracture mechanics*. Fracture and damage of concrete and rock, pp. 559–568.

Yang, Y., Liu, J. B., & Fan, J. S. (2016). Buckling behavior of double-skin composite walls: An experimental and modeling study. *Journal of Constructional Steel Research, 121*, 126–135

Zhao, G., Eligehausen, R. (1991). *Zugtragfähigkeit von Ankerplatten mit Kopfbolzen mit unterschiedlichen Achsabständen (Tensile capacity of anchor plates with headed bolts with different center distances)*. Bericht-Nr. KRT-799/07–91/23, Institut für Werkstoffe im Bauwesen, Universität Stuttgart.

Publisher's Note